Shape Control of Composite Plates and Shells with Embedded Actuators. I. Voltages Specified

DAVID B. KOCONIS, LÁSZLÓ P. KOLLÁR*
AND GEORGE S. SPRINGER
Department of Aeronautics and Astronautics
Stanford University
Stanford, CA 94305

(Received March 9, 1993)
(Revised August 9, 1993)

ABSTRACT: The changes in shapes of fiber-reinforced composite beams, plates and shells affected by embedded piezoelectric actuators were investigated. An analytical method was developed which can be used to calculate the changes in shapes for specified applied voltages to the actuators. The method is formulated on the basis of mathematical models using two-dimensional, linear, shallow shell theory including transverse shear effects which are important in the case of sandwich construction. Solutions to the governing equations were obtained via the Ritz method. A computationally efficient computer code with a user-friendly interface was written which is suitable for performing the numerical calculations. The code, designated as SHAPE1, provides the change in shape for specified applied voltages. To validate the method and the computer code, results generated by the code were compared to existing analytical and experimental results and to test data obtained during the course of the present investigation. The predictions provided by the SHAPE1 code were in excellent agreement with the results of the other analyses and data.

1. INTRODUCTION

IN RECENT YEARS great efforts have been made to build "smart" structures controlled by surface mounted and embedded piezoelectric actuators. Most of the past effort has been directed towards controlling the vibration characteristics of structures. Less work has been done on changing the shapes of structures, in spite of the fact that shape control is also a problem of practical interest. For example, embedded piezoelectric actuators could be used to adjust the shapes and the focal points of space antennas and the contours of aircraft, spacecraft, and ship control surfaces. However, to use piezoelectric actuators effectively, the type

*On leave from the Technical University of Budapest, Hungary.

0021-9983/94/05 415-44 $6.00/0

and locations of the actuators and the applied voltages must carefully be selected. This selection can best be accomplished by the use of analytical models.

During the course of this investigation two analytical models were developed which are applicable to two different types of problems (Figure 1). The first model is described in this paper, and is for calculating the changes in shapes of beams, plates and shells when the voltages applied to the piezoelectric actuators are given. The second model is presented in Reference [1], and is for determining the voltages needed to achieve a prescribed shape.

The literature on piezoelectric actuators attached to structural elements made of continuous fiber-reinforced composite materials falls broadly into two categories. In the first category are those investigations which primarily address dynamic (vibration) behavior of the structural element. In the second category are those studies which primarily deal with the "slow" (as opposed to dynamic) changes in shape produced by the piezoelectric actuators. Since these types of problems are the focus of this study, the literature on these latter types of investigations is reviewed briefly here. Crawley and de Luis [2,3], Bailey and Hubbard [4], Burke and Hubbard [5,6], Tzou and Wan [7,8], Cudney et al. [9–11], and Hanagud et al. [12] analyzed straight beams using methods based on the Bernoulli-Euler and Timoshenko beam theories. Crawley and Lazarus [13], Lee et al. [14–17], and Wang and Rogers [18,19] developed solution techniques for rectangular composite plates by modifying the classical laminate plate theory to allow for plies with induced strain. Tzou et al. [20–23] and Jia and Rogers [24] proposed methods for thin shells based on the Kirchhoff-Love shell theory. Ha et al. [25] and Tzou and Tseng [26,27], respectively, presented three-dimensional finite element solutions for flat rectangular plates and for plates with curved boundaries.

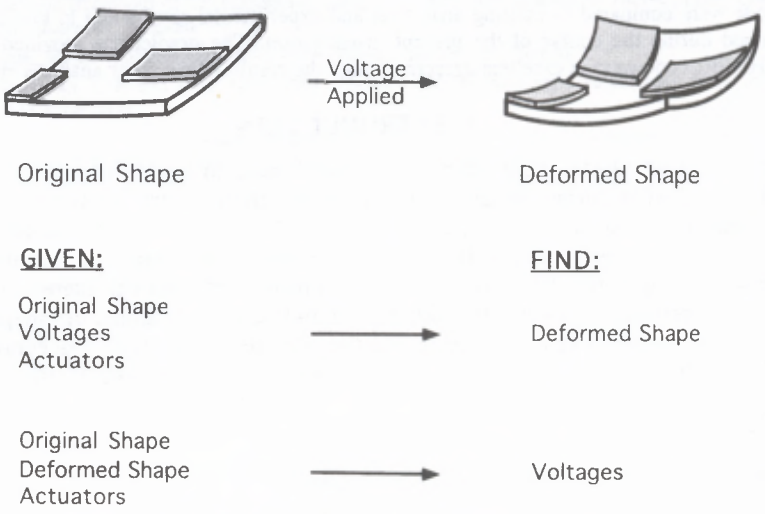

Figure 1. *Illustration of the problems considered in this investigation.*

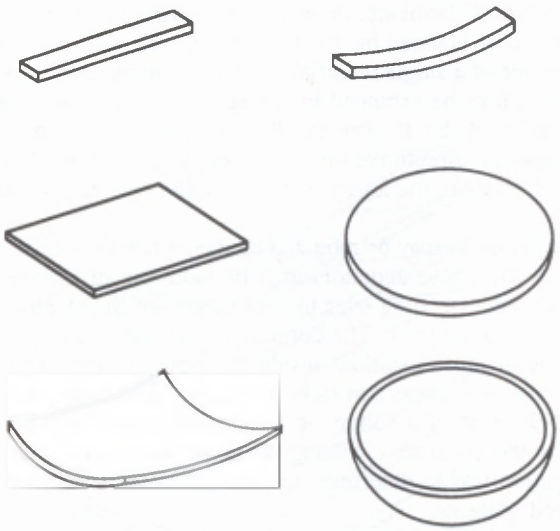

Figure 2. *Structural elements considered.*

None of the above investigators considered sandwich construction. Only the analyses of Tzou and Tseng [26,27] and Wada et al. [28–30] are applicable to shells of sandwich construction with a core undergoing shear deformation. Tzou and Tseng developed a three-dimensional finite element method which, in principle, could be applied to sandwich plates or shells but, to date, results have been reported only for solid isotropic cylindrical shells not containing a core. Wada et al. applied the commercial NASTRAN code to analyze the particular problem of a hexagonal sandwich plate. The model used in this study does not rely on finite element computations, and the result is shorter computing times and reduced memory requirements.

2. PROBLEM STATEMENT

Here we consider the problem in which a known set of voltages is applied to the piezoelectric actuators of a structure with a given shape and actuator configuration (Problem 1 in Figure 1). It is desired to find the change in shape caused by the strains induced by these applied voltages. This type of information is needed in designing piezoelectric actuator systems, namely in determining the types, shapes, and locations of actuators for efficient shape control.

We consider six different structural elements: (1) straight beam, (2) curved beam, (3) rectangular plate, (4) circular plate, (5) rectangular shell, and (6) circular shell (Figure 2). The element considered may be supported along any of its edges or at one or more locations on the top and bottom surfaces. The supports may be "built-in," "fixed" or "hinged," as illustrated in Figure 3. Each of these ele-

ments may be a "solid" laminate, or may be of sandwich construction consisting of an orthotropic core covered by two face sheets. The solid laminate or the face sheets may be made of a single material or of different materials bonded together. The layers (plies) may be arranged in any sequence, and the thicknesses of the layers may be different. Each layer may be isotropic or orthotropic, the latter including continuous unidirectional fiber-reinforced composites. Perfect bonding is assumed to exist between the layers themselves and between the face sheets and the core.

Piezoelectric actuators may be mounted on the surfaces or embedded inside the material (Figure 4). These actuators may be isotropic or orthotropic and may either be continuous extending over the entire area of the element, or they may be applied in discrete patches. The continuous actuators may be located on the surface or at one or more locations inside the material. Rectangular or circular patches of arbitrary thickness can only be on the top or bottom surfaces.

Upon the application of a voltage to each piezoelectric actuator, the actuator exerts a force on the material, changing the shape of the structure. The objective of this investigation was to determine the new shape of a structural element for specified applied voltages.

The shape of the element is described via a suitably chosen "reference" surface. The shape of this reference surface is defined by a single z_o-coordinate of every point on the surface, as illustrated in Figure 5. Note that the z_o-coordinate is perpendicular to an x-y plane. The shape must be such that the z_o-coordinate of every point can be specified by a polynomial function in x and y

$$z_o = \sum a_i x^{n_i} y^{m_i} \tag{1}$$

where a_i are constants and m_i and n_i are integers equal to or greater than zero.

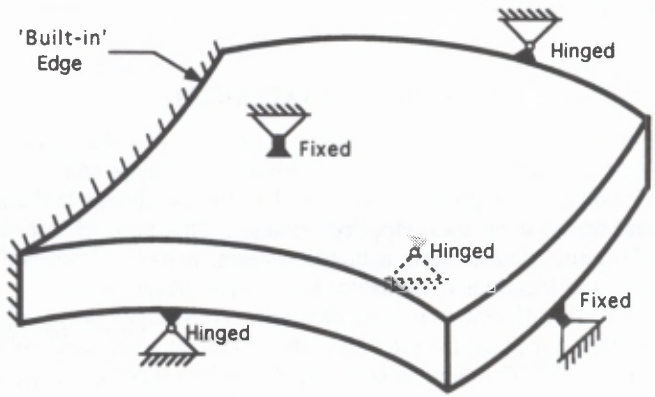

Figure 3. *Illustrations of the built-in, fixed and hinged supports.*

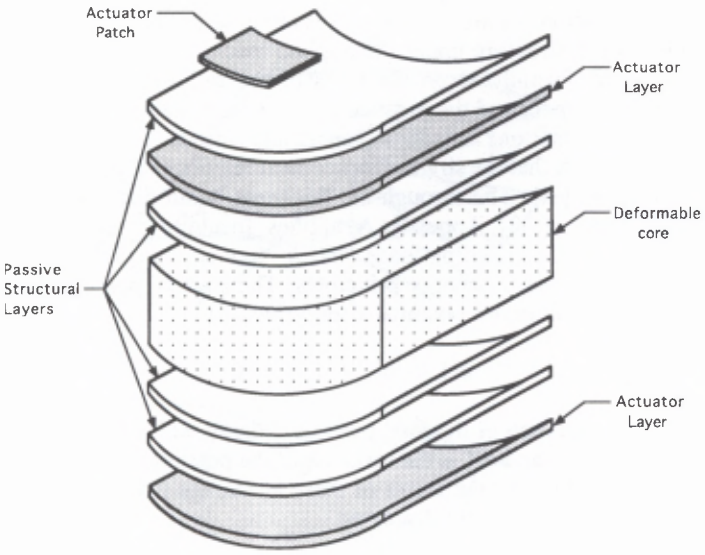

Figure 4. *Possible locations of continuous and discrete "patch" actuators.*

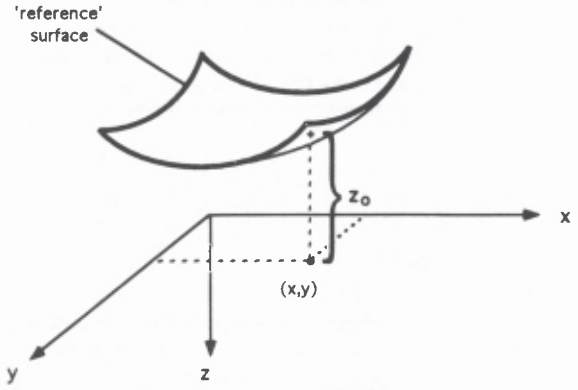

Figure 5. *z-coordinate describing the location of a point on the element reference surface.*

3. METHOD OF ANALYSIS

In this section we consider the problem in which the geometry of the structural element containing the piezoelectric actuators as well as the voltages applied to the piezoelectric actuators are specified. It is required to find the change in shape (new shape) of the structure under the applied loads.

The analysis is formulated on the basis of the following assumptions. The materials of the element and the piezoelectric actuators behave in linearly elastic manners. The deformations are small. The middle surface of the element is either flat or "shallow" such that the strain-displacement relations of flat plate or shallow shell theory apply [31]. The through-the-thickness strain distributions are such that sandwich theory ([32], Appendix A) applies. In addition, the face sheets may carry both in-plane and bending loads ("thick" face sheets, [32]).

The solution is based on energy principles. The starting point of the analysis is the principle of minimum potential energy [34,35]

$$\delta\Pi = \delta U + \delta V_e = 0 \tag{2}$$

where $\delta\Pi$ is the variation of the total potential energy, δU is the variation of the internal strain energy, and δV_e is the variation of the potential of the applied external forces. Before defining the forms of these terms, the displacements, strains, and stresses in the element are discussed.

3.1 Element Displacements, Strains, and Stresses

The element domain Ω and the coordinate systems used are defined in Figure 6. x-y-z is the global coordinate system, while x_1-x_2-x_3 is the local ply coordinate system with x_1 in the direction parallel to the fibers and x_2 and x_3 perpendicular to the fibers. The change in shape of the structural element is defined by the displacement of a reference surface which is located at a distance q from the bottom surface of the element and by the rotations of the normal to this surface at every point. q is obtained from the geometry of the sandwich construction using the following expression (Figure 7)

$$q = \frac{t_b}{2} + \left(\frac{t_b}{t_t + t_b}\right) d \tag{3}$$

where t_b, t_t, and d are defined in the figure. The displacement of the reference surface can be described by the linear displacements u, v, and w of every point on the surface. In addition the transverse shear deformation of the sandwich can be described by the rotations ϕ_x and ϕ_y which are discussed subsequently. As is shown in Figure 8, for a cross section in the x-z plane, u is the displacement tangential to the reference surface in the off-axis x-z plane, w is the deflection normal to the reference surface, and ϕ_x is the rotation in the x-z plane of a line which was normal to the reference surface before any deformations occurred and which connects corresponding points on the middle surfaces of the upper and lower face sheets (dashed line a–d). v is the displacement tangential to the reference surface

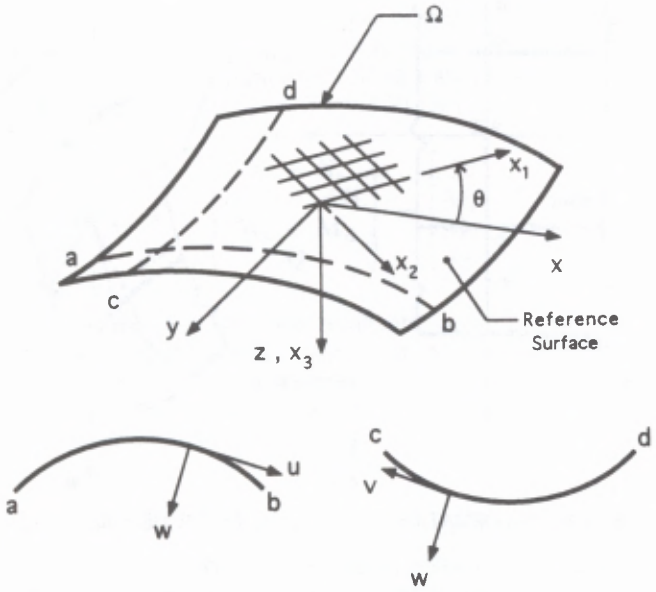

Figure 6. *Element domain and the global (x-y-z) and local ply (x_1-y_1-z_1) coordinate system.*

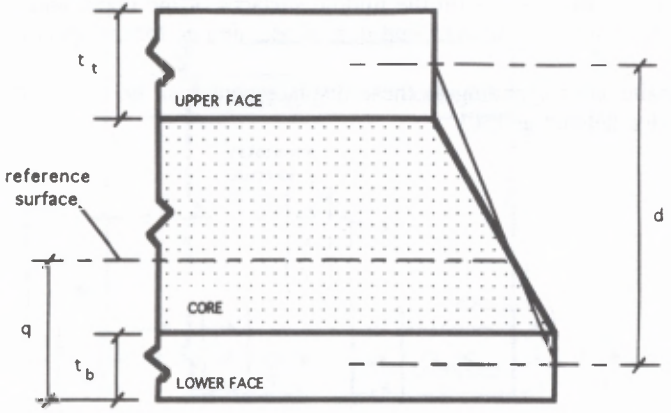

Figure 7. *Illustration of a deformed sandwich element showing the location of the reference surface.*

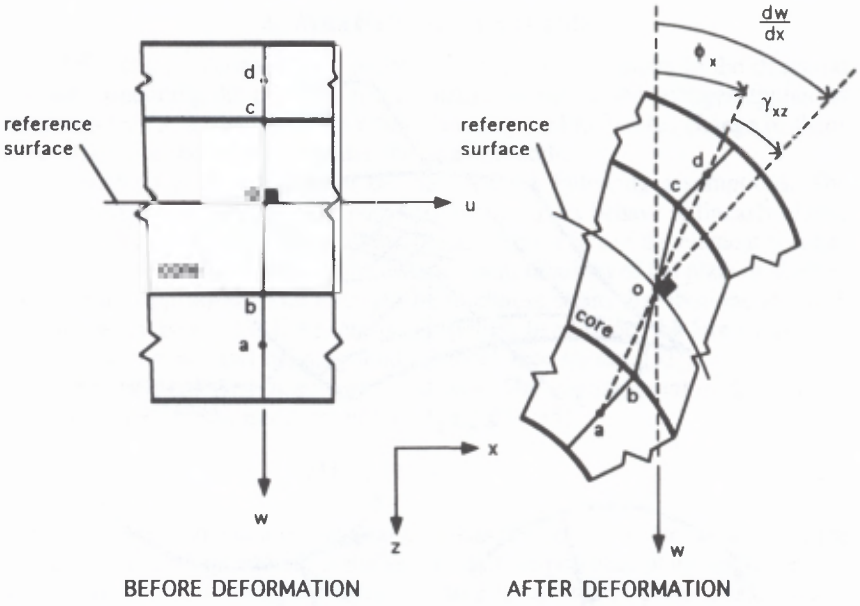

Figure 8. *Geometry of the element before and after deformation. Illustration of the shear deformation in the core which causes the straight normal a-b-o-c-d to become crooked.*

in the off-axis y-z plane, and ϕ_y is the rotation in the y-z plane of a line which was normal to the reference surface before any deformations occurred and which connects corresponding points on the middle surfaces of the upper and lower face sheets. The objective then is to find u, v, w, ϕ_x, and ϕ_y for the specified applied voltages.

The strains corresponding to these displacements can be represented by the strain vector defined as [36]

$$\epsilon = \begin{pmatrix} \epsilon_o \\ \varkappa_o \\ \varkappa \\ \gamma \end{pmatrix} \tag{4}$$

$$\epsilon_o = \begin{pmatrix} \epsilon_x \\ \epsilon_y \\ \epsilon_{xy} \end{pmatrix} \quad \varkappa_o = \begin{pmatrix} \varkappa_{o_x} \\ \varkappa_{o_y} \\ \varkappa_{o_{xy}} \end{pmatrix} \quad \varkappa = \begin{pmatrix} \varkappa_x \\ \varkappa_y \\ \varkappa_{xy} \end{pmatrix} \quad \gamma = \begin{Bmatrix} \gamma_{xz} \\ \gamma_{yz} \end{Bmatrix} \tag{5}$$

where ϵ_o represents the in-plane strains at the reference surface of the element, $\varkappa_o$ represents the "global" curvatures of the element in the presence of transverse shear deformation (obtained from ϕ_x and ϕ_y), $\varkappa$ represents the curvatures of the reference surface (obtained from w), and γ represents the transverse shear defor-

mations of the sandwich (Figure 8). These parameters are defined in Table 1. In this table, $z_o(x, y)$ is a function describing the original shape of the reference surface of the element before any deformation has occurred. If there is no core present, there is no transverse shear deformation; $\boldsymbol{\varkappa}_o$ and $\boldsymbol{\varkappa}$ are identical and $\boldsymbol{\gamma}$ is zero.

The internal forces corresponding to the strain $\boldsymbol{\epsilon}$ are represented by the following generalized force resultant vector (Figure 9) [36]

$$\mathbf{F} = \begin{pmatrix} \mathbf{N}_t + \mathbf{N}_b \\ d_b\mathbf{N}_b - d_t\mathbf{N}_t \\ \mathbf{M}_{l_t} + \mathbf{M}_{l_b} \\ \mathbf{Q} \end{pmatrix} = \begin{pmatrix} \mathbf{N} \\ \mathbf{M}_o \\ \mathbf{M}_l \\ \mathbf{Q} \end{pmatrix} \tag{6}$$

where $\mathbf{N}$ represents the in-plane stress resultants, which are the sum of the in-plane stress resultants of the top ($\mathbf{N}_t$) and bottom ($\mathbf{N}_b$) face sheets, $\mathbf{M}_o$ the global moment resultants, $\mathbf{M}_l$ the local moment resultants, which are the sum of the moment resultants carried by the local bending of the top ($\mathbf{M}_{l_t}$) and bottom ($\mathbf{M}_{l_b}$) face sheets, and $\mathbf{Q}$ the shear stress resultants. The forms of these stress resultants are

$$\mathbf{N} = \begin{pmatrix} N_x \\ N_y \\ N_{xy} \end{pmatrix} \quad \mathbf{M}_o = \begin{pmatrix} M_{o_x} \\ M_{o_y} \\ M_{o_{xy}} \end{pmatrix} \quad \mathbf{M}_l = \begin{pmatrix} M_{l_x} \\ M_{l_y} \\ M_{l_{xy}} \end{pmatrix} \quad \mathbf{Q} = \begin{Bmatrix} Q_{xz} \\ Q_{yz} \end{Bmatrix} \tag{7}$$

d_t and d_b are, respectively, the distances from the reference surface to the middle surfaces of the top and bottom face sheets (Figure 9).

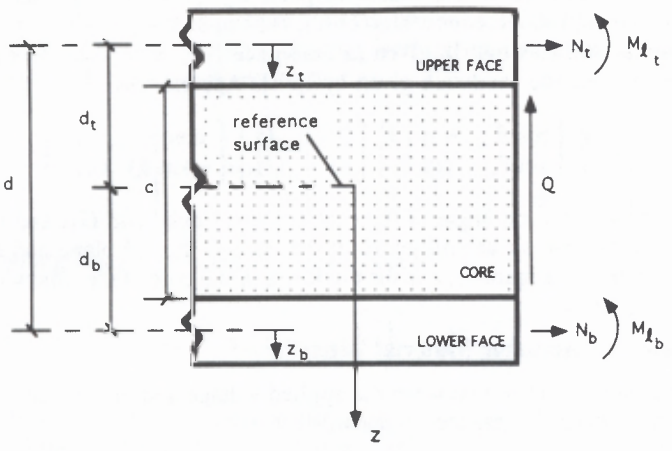

Figure 9. *Force and moment resultants and cross section dimensions for the sandwich element.*

Table 1. Strain vector definitions.

Vector	Components		
ϵ_o	$\epsilon_x = \frac{\partial u}{\partial x} - w\frac{\partial^2 z_o}{\partial x^2}$	$\epsilon_y = \frac{\partial v}{\partial y} - w\frac{\partial^2 z_o}{\partial y^2}$	$\gamma_{xy} = \frac{\partial u}{\partial y} + \frac{\partial v}{\partial x} - 2w\frac{\partial^2 z_o}{\partial x \partial y}$
$\varkappa_o$	$\varkappa_{ox} = -\frac{\partial \phi_x}{\partial x}$	$\varkappa_{oy} = -\frac{\partial \phi_y}{\partial y}$	$\varkappa_{oxy} = -\frac{\partial \phi_x}{\partial y} - \frac{\partial \phi_y}{\partial x}$
$\varkappa$	$\varkappa_x = -\frac{\partial^2 w}{\partial x^2}$	$\varkappa_y = -\frac{\partial^2 w}{\partial y^2}$	$\varkappa_{xy} = -2\frac{\partial^2 w}{\partial x \partial y}$
γ	$\gamma_{xz} = \frac{\partial w}{\partial x} - \phi_x$	$\gamma_{yz} = \frac{\partial w}{\partial y} - \phi_y$	

The generalized forces and the strains are related through the expression

$$\mathbf{F} = \mathbf{S}\epsilon \tag{8}$$

where $\mathbf{S}$ is the stiffness matrix (Appendix A)

$$\mathbf{S} = \begin{bmatrix} \mathbf{A}_b + \mathbf{A}_t & d_b\mathbf{A}_b - d_t\mathbf{A}_t & \mathbf{B}_b + \mathbf{B}_t & \mathbf{0} \\ d_b\mathbf{A}_b - d_t\mathbf{A}_t & d_b^2\mathbf{A}_b + d_t^2\mathbf{A}_t & d_b\mathbf{B}_b - d_t\mathbf{B}_t & \mathbf{0} \\ \mathbf{B}_b + \mathbf{B}_t & d_b\mathbf{B}_b - d_t\mathbf{B}_t & \mathbf{D}_b + \mathbf{D}_t & \mathbf{0} \\ \mathbf{0} & \mathbf{0} & \mathbf{0} & \mathbf{G} \end{bmatrix} \tag{9}$$

In Equation (9), $\mathbf{A}$, $\mathbf{B}$, and $\mathbf{D}$ are the Classical Laminated Plate Theory stiffness matrices for the face sheet about its own middle surface. The subscripts t and b refer to the top and bottom face sheets, respectively. As shown in Appendix A, for a solid element (which contains no core), the upper left portion of $\mathbf{S}$ reduces to the classical stiffness matrix given in Reference [37]. $\mathbf{G}$ is the off-axis shear stiffness matrix for the sandwich given by ([32], Appendix A)

$$\mathbf{G} = \frac{d^2}{c}\begin{bmatrix} \cos\theta & -\sin\theta \\ \sin\theta & \cos\theta \end{bmatrix}\begin{bmatrix} G_{13}^c & 0 \\ 0 & G_{23}^c \end{bmatrix}\begin{bmatrix} \cos\theta & \sin\theta \\ -\sin\theta & \cos\theta \end{bmatrix} \tag{10}$$

where θ is the orientation angle of the core principal axis, and G_{13}^c and G_{23}^c are the on-axis transverse shear stiffnesses of the core in the 1-3 plane and the 2-3 planes, respectively (Figure 6). c is the thickness of the core of the sandwich construction (Figure 9).

3.2 Piezoelectric Actuator Material Behavior

The simplest relationship between the applied voltage and the induced electric strain in a piezoelectric material is linear, i.e.

$$\epsilon_{el} = \hat{\mathbf{d}}\left(\frac{e}{t}\right) \tag{11}$$

where e is the voltage applied across the material, t is the thickness of the material, and $\hat{\mathbf{d}}$ is the vector of the on-axis piezoelectric strain constants [3]. However, when a voltage is applied across certain piezoelectric materials (such as piezoceramics), they exhibit a nonlinear strain response [13]. It has been proposed [13] that this response is due to the fact that the components of $\hat{\mathbf{d}}$ are not constant, but vary with the applied voltage or the strain present in the piezoelectric material [13]. In this case the induced electrical strain versus voltage relationship may be expressed as

$$\boldsymbol{\epsilon}_{el} = \hat{\mathbf{d}}(e,\boldsymbol{\epsilon}_t)\left(\frac{e}{t}\right) \tag{12}$$

where $\boldsymbol{\epsilon}_t$ is the vector of total in-plane strains present in the piezoelectric material. We can now approximate $\hat{\mathbf{d}}(e,\boldsymbol{\epsilon}_t)$ by

$$\hat{\mathbf{d}}(e,\boldsymbol{\epsilon}_t) = \mathbf{d}_o + \boldsymbol{\chi}\left(\frac{e}{t}\right) + \boldsymbol{\psi}\boldsymbol{\epsilon}_t \tag{13}$$

where $\mathbf{d}_o$, $\boldsymbol{\chi}$, and $\boldsymbol{\psi}$ represent the on-axis properties of the piezoelectric material. The components of $\mathbf{d}_o$, $\boldsymbol{\chi}_o$, and $\boldsymbol{\psi}$ for an orthotropic piezoelectric material are

$$\mathbf{d}_o = \begin{Bmatrix} \hat{d}_{31} \\ \hat{d}_{32} \\ 0 \end{Bmatrix} \quad \boldsymbol{\chi} = \begin{Bmatrix} \chi_{31} \\ \chi_{32} \\ 0 \end{Bmatrix} \quad \boldsymbol{\psi} = \begin{bmatrix} \psi_1 & \psi_2 & 0 \\ \psi_2 & \psi_3 & 0 \\ 0 & 0 & \psi_4 \end{bmatrix} \tag{14}$$

The values of these properties must be determined experimentally for the piezoelectric material (e.g., [13]). The above piezoelectric properties are in the on-axis coordinate system. In the off-axis coordinate system we denote these properties by $\bar{\mathbf{d}}$, $\bar{\boldsymbol{\chi}}$, and $\bar{\boldsymbol{\psi}}$. These off-axis properties can be obtained by the usual coordinate transformations. For an isotropic piezoelectric material, the components of $\mathbf{d}_o$, $\boldsymbol{\chi}$, and $\boldsymbol{\psi}$ reduce to

$$\mathbf{d}_o = \begin{Bmatrix} \hat{d}_{31} \\ \hat{d}_{31} \\ 0 \end{Bmatrix} \quad \boldsymbol{\chi} = \begin{Bmatrix} \chi_{31} \\ \chi_{31} \\ 0 \end{Bmatrix} \quad \boldsymbol{\psi} = \begin{bmatrix} \psi_1 & \psi_2 & 0 \\ \psi_2 & \psi_1 & 0 \\ 0 & 0 & \psi_2 - \psi_1 \end{bmatrix} \tag{15}$$

By combining Equations (13) and (11) we obtain

$$\boldsymbol{\epsilon}_{el} = \mathbf{d}_o\left(\frac{e}{t}\right) + \boldsymbol{\chi}\left(\frac{e}{t}\right)^2 + \boldsymbol{\psi}\boldsymbol{\epsilon}_t\left(\frac{e}{t}\right) \tag{16}$$

The stress present in a piezoelectric material $\boldsymbol{\sigma}_p$ can be related to the total strains and the electrical strains as follows [13]

$$\boldsymbol{\sigma}_p = \mathbf{S}_p(\boldsymbol{\epsilon}_t - \boldsymbol{\epsilon}_{el}) \tag{17}$$

where $\mathbf{S}_p$ is the stiffness matrix of the piezoelectric material which has the usual form associated with an orthotropic material. By substituting Equation (16) into Equation (17) and rearranging terms we obtain

$$\sigma_p = \mathbf{S}_p^* \epsilon_t - \mathbf{S}_p \left(\mathbf{d}_o \left(\frac{e}{t} \right) + \chi \left(\frac{e}{t} \right)^2 \right) \tag{18}$$

where $\mathbf{S}_p^*$ is a modified stiffness matrix

$$\mathbf{S}_p^* = \left(\mathbf{I} - \psi \left(\frac{e}{t} \right) \right) \mathbf{S}_p \tag{19}$$

and $\mathbf{I}$ is the 3×3 identity matrix. Inspection of Equations (18) and (19) reveals that for a specified applied voltage e and applied stress σ_p, the total strain ϵ_t in a piezoelectric material may in fact be determined directly, without the need of iteration.

3.3 Internal Strain Energy

Having defined the stresses and strains in the element, we may now express the variation of the strain energy δU in Equation (2) as [38]

$$\delta U = \delta \left(\frac{1}{2} \int\int_{\Omega} (\epsilon^T \mathbf{S}^* \epsilon - 2\epsilon^T \mathbf{F}_{el}^*) dA \right) \tag{20}$$

where $[\ ]^T$ represents the transpose of a matrix or vector and $\mathbf{S}^*$ represents a modified stiffness matrix which has the form

$$\mathbf{S}^* = \mathbf{S} - 2\mathbf{S}_{el1} + \mathbf{S}_{el2} \tag{21}$$

$\mathbf{S}_{el1}$ and $\mathbf{S}_{el2}$ are the contributions due to the nonlinear piezoelectric material behavior [Equation (16)] and are identical in form to the stiffness matrix $\mathbf{S}$ given by Equation (9). However, when computing the $\mathbf{A}$, $\mathbf{B}$, and $\mathbf{D}$ matrices in this equation, only the piezoelectric plies are included and the off-axis ply stiffness matrix for the kth piezoelectric ply, $\mathbf{Q}^k$, is replaced by $(\mathbf{Q}\bar{\psi}(e/t))^k$ in the case of $\mathbf{S}_{el1}$ and by $(\bar{\psi}^T \mathbf{Q} \bar{\psi}(e/t)^2)^k$ in the case of $\mathbf{S}_{el2}$.

In Equation (20), $\mathbf{F}_{el}^*$ represents the generalized electrical force vector which results from the application of a voltage assuming deformation is restricted. $\mathbf{F}_{el}^*$ has the form

$$\mathbf{F}_{el}^* = \mathbf{F}_{el1} + \mathbf{F}_{el2} + \mathbf{F}_{el3} \tag{22}$$

$\mathbf{F}_{el1}$ is expressed as

$$\mathbf{F}_{el1} = \begin{pmatrix} \mathbf{N}_{el1} \\ \mathbf{M}_{o_{el1}} \\ \mathbf{M}_{l_{el1}} \\ \mathbf{0} \end{pmatrix} \tag{23}$$

where $\mathbf{N}_{el1}$ represents in-plane electrical stress resultants, $\mathbf{M}_{o_{el1}}$ global electrical moment resultants, and $\mathbf{M}_{l_{el1}}$ local electrical moment resultants carried by the local bending of the upper (t) and lower (b) face sheets. The final entry in $\mathbf{F}_{el1}$ is a 2×1 vector of zeros indicating that the application of voltages produces no transverse shear stress resultant. The equations for the three stress and moment vectors are [37]

$$\mathbf{N}_{el1} = \begin{Bmatrix} N_{el1_x} \\ N_{el1_y} \\ N_{el1_{xy}} \end{Bmatrix} = \sum_{k=1}^{n_{el}} \mathbf{Q}^k \bar{\mathbf{d}}^k e^k \tag{24}$$

$$\mathbf{M}_{o_{el1}} = \begin{Bmatrix} M_{o_{el1_x}} \\ M_{o_{el1_y}} \\ M_{o_{el1_{xy}}} \end{Bmatrix} = d_b \left(\sum_{k=1}^{n_{elb}} \mathbf{Q}^k \bar{\mathbf{d}}^k e^k \right) - d_t \left(\sum_{k=1}^{n_{elt}} \mathbf{Q}^k \bar{\mathbf{d}}^k e^k \right) \tag{25}$$

$$\mathbf{M}_{l_{el1}} = \begin{Bmatrix} M_{l_{el1_x}} \\ M_{l_{el1_y}} \\ M_{l_{el1_{xy}}} \end{Bmatrix} = \sum_{k=1}^{n_{elt}} \mathbf{Q}^k \bar{\mathbf{d}}^k e^k \left(z_t^k + \frac{t^k}{2} \right) + \sum_{k=1}^{n_{elb}} \mathbf{Q}^k \bar{\mathbf{d}}^k e^k \left(z_b^k + \frac{t^k}{2} \right) \tag{26}$$

where $\mathbf{Q}^k$ is the off-axis ply stiffness matrix for the kth ply, and n_{el}, n_{elt}, and n_{elb} are the total number of piezoelectric plies, the number of piezoelectric plies in the upper face sheet, and the number of piezoelectric plies in the lower face sheet, respectively. z_t^k and z_b^k are the z-coordinates of the top surface of the kth ply as measured from the middle surface of the upper and lower face sheets, respectively (Figure 9).

The remaining terms on the left side of Equation (22), $\mathbf{F}_{el2}$ and $\mathbf{F}_{el3}$ are identical in form to $\mathbf{F}_{el1}$ given by Equation (23). However when computing the $\mathbf{N}_{el}$, $\mathbf{M}_{o_{el}}$, and $\mathbf{M}_{l_{el}}$ in Equations (24) through (26), $\mathbf{Q}^k$ is replaced by $(\bar{\Psi}^T \mathbf{Q}(e/t))^k$ in the case of $\mathbf{F}_{el2}$ and $\bar{\mathbf{d}}^k$ is replaced by $(\bar{\chi}(e/t))^k$ in the case of $\mathbf{F}_{el3}$.

3.4 Potential of External Forces

The variation of the potential of the applied external forces δV_e may be expressed as [35]

$$\delta V_e = \delta V_{BC} + \delta V'_{BC} \tag{27}$$

δV_{BC} represents the variation of energy that would be stored in the supports restraining the element if the supported boundary locations were elastic. $\delta V'_{BC}$ represents the variation of energy that would be stored in "fictitious" supports employed to prevent rigid body motion.

3.4.1 POTENTIAL OF SUPPORTS $\delta \mathrm{V_{BC}}$

The external forces considered here are introduced via the element supports. The displacements at the supports are defined to be zero, which implies that no energy may be stored. However, this constraint is enforced using a penalty

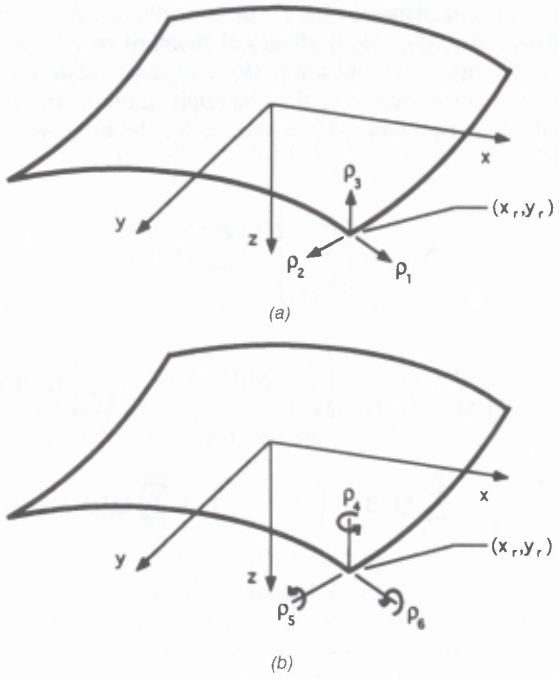

Figure 10. *Displacement directions for the supports at* (x_r, y_r)*: (a) linear displacements and (b) rotations.*

method as follows. At a given support (denoted by the subscript r) the energy stored δV_{BC_r} may be expressed [39]

$$\delta V_{BC_r} = \delta\left(\frac{1}{2}\sum_{i=1}^{6}\lambda_i \varrho_i^2\right) \tag{28}$$

ϱ_1 through ϱ_3 and ϱ_4 through ϱ_6 represent, respectively, linear and angular displacements at the support considered (Figure 10)

$$\begin{aligned} \varrho_1 &= u(x_r, y_r) & \varrho_4 &= \left(\frac{\partial v}{\partial x}\right)_{(x_r, y_r)} \\ \varrho_2 &= v(x_r, y_r) & \varrho_5 &= \left(\frac{\partial w}{\partial x}\right)_{(x_r, y_r)} \\ \varrho_3 &= w(x_r, y_r) & \varrho_6 &= \left(\frac{\partial w}{\partial y}\right)_{(x_r, y_r)} \end{aligned} \tag{29}$$

(x_r, y_r) are the coordinates of the support. Note that if a support is applied on the top or bottom surface, the displacements at that support must be expressed in terms of the displacements at the corresponding location on the reference surface (see Section 3.5). λ_i is a penalty multiplier corresponding to each of these displacements. The value of λ reflects the magnitude of the permissible boundary displacement. At a fixed support no linear or angular displacements are permitted, while at a hinged support only angular displacements are permitted. For permissible displacements the corresponding value of λ is set equal to zero. If a displacement is not permitted, the corresponding λ is set to a high value. As with all penalty multiplier methods, care must be taken to use a value of λ that is not so large as to cause the problem to become ill-conditioned. It was found that the value of $\lambda_i = 1 \times 10^7$ results in satisfactory solutions for the problems analyzed in this investigation.

Equation (28) must be applied at every support. Thus δV_{BC} is the sum of all the δV_{BC_r}

$$\delta V_{BC} = \delta\left(\sum_{supports} \delta V_{BC_r} \right) \tag{30}$$

A built-in support is approximated by a number of adjoining discrete fixed supports.

3.4.2 POTENTIAL OF FICTITIOUS SUPPORTS $\delta V'_{BC}$

By applying a voltage to the piezoelectric actuators the element cannot undergo rigid body motion, it can only change its shape. However, the solution technique employed here relies on assumed functions for the displacements. The forms of these functions are general and may result in solutions which include rigid body motions. These rigid body motions are removed from the solution by forcing selected displacements of the new and original shapes to match. This removal is accomplished by the following procedure.

Nonpermissible rigid body motion appears in the solution under three typical circumstances: (1) the element is not restrained at any point, (2) the element is hinged at one point only, or (3) the element is hinged at two or more points, these points being at colinear locations (Figure 11). In the first case, the rigid body motion is eliminated by adding a fictitious support which prevents three rotations and three displacements [ϱ_1 through ϱ_6 in Equation (29)] at some reference point. In the second case, the rigid body motion is eliminated by adding a fictitious support which prevents three rotations (ϱ_4 through ϱ_6) about the actual support point. In the third case, the rigid body motion is eliminated by adding a fictitious support which prevents rotation (either ϱ_4, ϱ_5, or ϱ_6) about the line containing the actual colinear hinges.

The variation of the potential energy at the fictitious supports $\delta V'_{BC}$ is then calculated analogous to δV_{BC} [see Equation (30)].

3.5 Displacements and Strains throughout the Element

The above analysis is formulated using the displacements and strains at the ref-

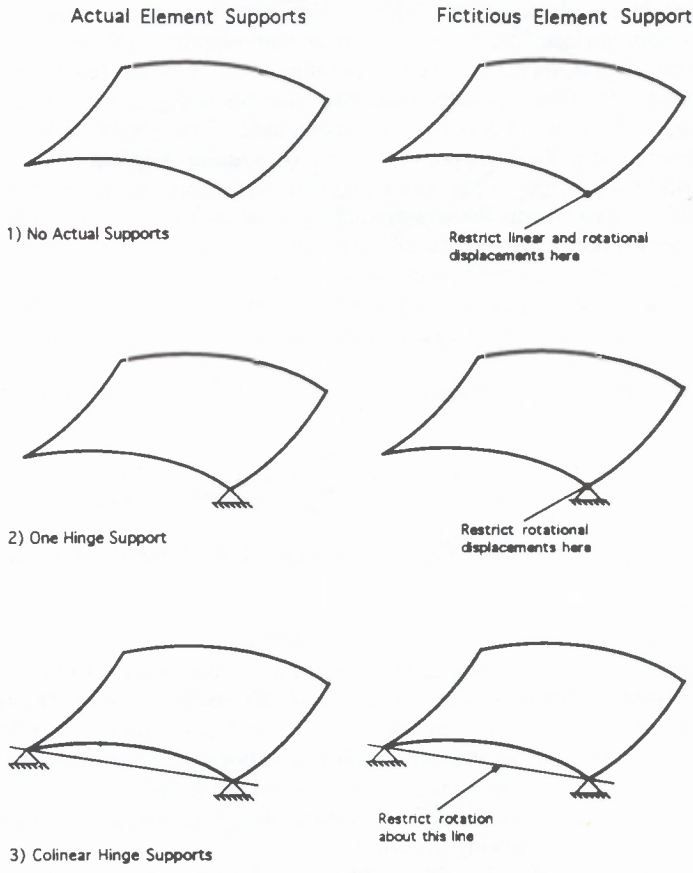

Figure 11. *Possible support conditions requiring fictitious supports.*

erence surface. It may be required to determine the displacements and strains at other locations through the thickness of the element. For example, if there is a support applied on the top or bottom surface as mentioned in Section 3.4.1, the displacement at the top or bottom surface of the element must be expressed in terms of the displacements at the reference surface. To express the displacement anywhere in the element, the element is divided into three regions: (1) the top face sheet, (2) the bottom face sheet, and (3) the core. In each of these regions a different expression applies for the displacement. The expressions for the displacements u_p, v_p, and w_p of a point P in the element in each region are obtained by considering the geometry of the deformed cross section (Figure 12) and appear in Table 2. The in-plane strains ϵ_x, ϵ_y, and γ_{xy} at point P in the face sheets and core of the element may now be obtained by substituting the expressions in Table 2 into the corresponding expressions in Table 1. The shear strains in the

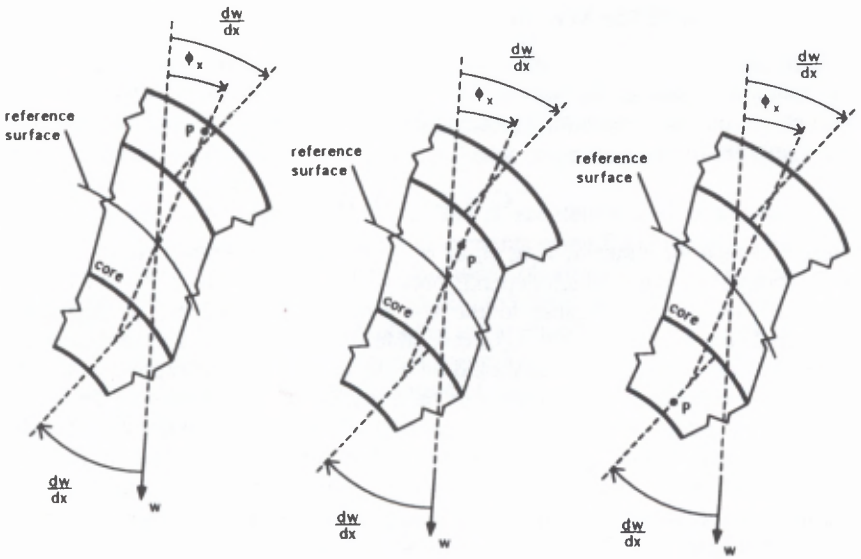

Figure 12. *Illustration of a deformed section of the element showing the point P in the top face sheet, the core, and the bottom face sheet.*

face sheets are zero, while those of the core, γ'_{xz} and γ'_{yz} defined in Appendix A, may be obtained by substituting the expressions in Table 2 into Equations (A.3) and (A.11).

4. METHOD OF SOLUTION

In this section we develop the solution to the equations developed in the previous section for the problem in which the geometry of the structural element containing the piezoelectric actuators as well as the voltages applied to the piezoelectric actuators are specified and it is required to find the change in shape (new shape) of the structure under the applied loads.

Table 2. Expressions relating the displacements throughout the element to the displacements at the reference surface.

	Top Face Sheet	Core	Bottom Face Sheet
u_p	$u + \phi_x d_t + z_t \dfrac{\partial w}{\partial x}$	$u + \phi_x z$	$u - \phi_x d_b + z_b \dfrac{\partial w}{\partial x}$
v_p	$v + \phi_y d_t + z_t \dfrac{\partial w}{\partial y}$	$v + \phi_y z$	$v - \phi_y d_b + z_b \dfrac{\partial w}{\partial y}$
w_p	w	w	w

4.1 Calculation of the New Shape

Calculation of the new shape requires that the displacements u, v, and w and the rotations ϕ_x and ϕ_y be known. As a first step in the solution, expressions are chosen for the displacements and rotations. These expressions can be written in the symbolic form

$$C = \Sigma c_i s_i(x, y) \tag{31}$$

Here C stands for either u, v, w, ϕ_x or ϕ_y. c_i are as yet unknown constants. s_i is a polynomial function which depends only on the in-plane off-axis x and y coordinates. Functions applicable to the six geometries considered in this study (Figure 2) are given in Table 3. In this table u_i, v_i, w_i, α_i and β_i represent the unknown constants. This table should be used as follows. The expressions given in Table 3 represent the functions to be used for straight beams or for plates (where z_o is a zero or first order polynomial) and for curved beams or for shells (where z_o is a second order polynomial). For surfaces described by third or higher order polynomials, the expressions for u and v must be modified. If z_o is a polynomial of order m, then $\mathbf{f}^{cb}$ or $\mathbf{f}^{s}$ and $\mathbf{g}^{s}$ (depending on whether the surface is a curved beam or a shell, respectively) should be of order $3 + (m - 2)$. Note that the table is for z_o which is a second order polynomial, in which case $m = 2$ and $\mathbf{f}^{cb}$, $\mathbf{f}^{s}$, and $\mathbf{g}^{s}$ are third order. Displacement functions selected in this manner are the minimum functions which insure that the inextensional deformations [40] are included. Omitting these deformations can produce errors in the calculations which may be several orders of magnitude.

Table 3. Suitable expressions for the displacements and rotations.

	u	v	w	ϕ_x	ϕ_y
Straight beam	$\sum_{i=1}^{3} u_i^{sb} f_i^{sb}$		$\sum_{i=1}^{6} w_i^{sb} h_i^{sb}$	$\sum_{i=1}^{3} \alpha_i^{sb} p_i^{sb}$	
Curved beam	$\sum_{i=1}^{10} u_i^{cb} f_i^{cb}$		$\sum_{i=1}^{6} w_i^{cb} h_i^{cb}$	$\sum_{i=1}^{3} \alpha_i^{cb} p_i^{cb}$	
Rectangular or circular plates	$\sum_{i=1}^{3} u_i^{p} f_i^{p}$	$\sum_{i=1}^{3} v_i^{p} g_i^{p}$	$\sum_{i=1}^{6} w_i^{p} h_i^{p}$	$\sum_{i=1}^{3} \alpha_i^{p} p_i^{p}$	$\sum_{i=1}^{3} \beta_i^{p} r_i^{p}$
Rectangular or circular shells	$\sum_{i=1}^{10} u_i^{s} f_i^{s}$	$\sum_{i=1}^{10} v_i^{s} g_i^{s}$	$\sum_{i=1}^{6} w_i^{s} h_i^{s}$	$\sum_{i=1}^{3} \alpha_i^{s} p_i^{s}$	$\sum_{i=1}^{3} \beta_i^{s} r_i^{s}$

$\mathbf{f}^{sb}, \mathbf{p}^{sb}, \mathbf{p}^{cb} = \{1, x\}$
$\mathbf{h}^{sb}, \mathbf{h}^{cb} = \{1, x, x^2\}$
$\mathbf{f}^{cb} = \{1, x, x^2, x^3\}$

$\mathbf{f}^{p}, \mathbf{g}^{p}, \mathbf{p}^{p}, \mathbf{r}^{p}, \mathbf{p}^{s}, \mathbf{r}^{s} = \{1, x, y\}$
$\mathbf{h}^{p}, \mathbf{h}^{s} = \{1, x, y, x^2, xy, y^2\}$
$\mathbf{f}^{s}, \mathbf{g}^{s} = \{1, x, y, x^2, xy, y^2, x^3, x^2y, xy^2, y^3\}$

The first set of calculations to determine the displacements (as described subsequently) should be done with **f**, **g**, **h**, **p**, and **r** as discussed above. However, in some cases higher order polynomials are required to achieve accurate results. Therefore, the order of **f**, **g**, **h**, **p**, and **r** should be increased, and the calculations repeated. The resulting displacements should be compared with those obtained previously. When no significant improvement is obtained, the calculations are stopped.

The unknown constants u_i, v_i, w_i, α_i and β_i are determined as follows. The strains are expressed in terms of the displacements using Equation (4). The electrical force vector is evaluated using Equations (24) through (26). The resulting expressions are substituted into Equation (20) to obtain the variation of the strain energy δU. The variation of the potential of the applied external forces δV_e is then expressed in terms of the displacements using Equation (27). After performing these algebraic manipulations, the variation of minimum potential energy [Equation (2)] becomes

$$\delta\Pi(\bar{\mathbf{C}}) = \delta(\bar{\mathbf{C}}^T(\mathbf{R}_1 + \mathbf{R}_{sup})\bar{\mathbf{C}} + \mathbf{R}_2\bar{\mathbf{C}}) \tag{32}$$

where $\bar{\mathbf{C}}$ is the vector of the unknown constants

$$\bar{\mathbf{C}} = \begin{Bmatrix} \mathbf{u} \\ \mathbf{v} \\ \mathbf{w} \\ \alpha \\ \beta \end{Bmatrix}$$

and $\mathbf{R}_1$, $\mathbf{R}_2$, and $\mathbf{R}_{sup}$ are defined in Table 4. In this table $\mathbf{T}_{ue}$ is the transformation matrix which gives the combined strain vector ϵ when multiplied by $\bar{\mathbf{C}}$, i.e.

$$\epsilon = \mathbf{T}_{ue}\bar{\mathbf{C}} \tag{33}$$

The actual expression for this transformation matrix is in Appendix B.

The unknown constants $\bar{\mathbf{C}}$ are then evaluated from

$$\frac{\partial\Pi}{\partial\bar{C}_i} = 0 \tag{34}$$

The result is

$$\bar{\mathbf{C}} = (\mathbf{R}_1 + \mathbf{R}_1^T + \mathbf{R}_{sup} + \mathbf{R}_{sup}^T)^{-1}\mathbf{R}_2 \tag{35}$$

It is important to note that Equation (35) is a linear set of algebraic equations. Hence $\bar{\mathbf{C}}$ can be found in a straightforward manner (without the need for iteration) even though the piezoelectric material may behave nonlinearly with respect to the applied voltage. This linearity of the equation results in simpler and faster solutions than the procedures employed previously for problems with a similar type of material behavior [13].

Table 4. Definitions of terms appearing in Equation (34).

Term	Origin	Definition
$\mathbf{R}_1$	total strains	$\frac{1}{2}\iint_{\Omega} \mathbf{T}_{ue}^T \mathbf{S}^* \mathbf{T}_{ue}\, dxdy$
$\mathbf{R}_2$	electrical strains	$-\iint_{\Omega} \mathbf{T}_{ue}^T \mathbf{F}_{el}^*\, dxdy$
$\mathbf{R}_{sup}$	energy of the supports	(see below)

For all three displacements and all three rotations supported at (x_r, y_r)

$$\mathbf{R}_{sup} = \begin{bmatrix} \lambda_1 \mathbf{f}^T\mathbf{f} & 0 & 0 & 0 \\ 0 & \lambda_2 \mathbf{g}^T\mathbf{g} + \lambda_3 \frac{\partial \mathbf{g}^T}{\partial x}\frac{\partial \mathbf{g}}{\partial x} & 0 & 0 \\ 0 & 0 & \lambda_4 \mathbf{h}^T\mathbf{h} + \lambda_5 \frac{\partial \mathbf{h}^T}{\partial x}\frac{\partial \mathbf{h}}{\partial x} + \lambda_6 \frac{\partial \mathbf{h}^T}{\partial y}\frac{\partial \mathbf{h}}{\partial y} & 0 \\ 0 & 0 & 0 & 0 \end{bmatrix}_{(x_r, y_r)}$$

From the known values of $\overline{\mathbf{C}}$, the displacements and strains at the reference surface may be calculated from the expressions given in Tables 3 and 1. The displacements and strains at other locations can be calculated from the relationships in Section 3.5. The stresses may be obtained using stress-strain relations found in Reference [37].

It is noted that changes in the temperature may also result in a change of shape. The effects of temperature are included in Reference [33].

4.2 Numerical Implementation

Solutions to the aforementioned equations must be obtained by numerical means. To generate numerical results, a user-friendly computer code designated as SHAPE1 was written. Two points must be mentioned regarding the numerical implementation. The calculations require that the integrals

$$\frac{1}{2}\iint_{\Omega} \mathbf{T}_{ue}^T \mathbf{S}^* \mathbf{T}_{ue}\, dx\, dy, \qquad \iint_{\Omega} \mathbf{T}_{ue}^T \mathbf{F}_{el}^*\, dx\, dy \tag{36}$$

be evaluated over the entire domain Ω (see Table 4), where $\mathbf{S}^*$ and $\mathbf{F}_{el}^*$ are known functions of x and y. For a rectangular domain the integration can be performed using Simpson's rule [41]. For a circular domain Simpson's rule had to be modified, and the integration procedure is described in Reference [33].

In the numerical calculation of the above integrals, the functions $\mathbf{S}^*$ and $\mathbf{F}_{el}^*$ are evaluated at a prescribed number of designated (x, y) locations, called integration points (Figure 13). The locations of these points are specified by the number of divisions chosen in the x- and y-directions. The values of these functions depend on the stiffness and on the electric force applied to the element at the integration point. The stiffness and electric force at an integration point depend, in turn, on whether or not there is a patch at that point and whether the patch is located on the top or bottom surface of the element. Therefore, at each integration point, the stiffness matrix and the electric force vector are the sum of the stiffness and electric force of every layer in the substrate of the element plus the stiffness and electric force of the corresponding patches covering that point (Figure 13).

5. VERIFICATION

In order to validate the model and the SHAPE1 computer code, results calculated by the code were compared to other analytical, numerical, and experimental results. The following five problems were included in these comparisons:

1. Cantilever, straight, sandwich beam
2. Cantilever, straight beam made of two continuous piezoelectric layers
3. Flat, rectangular, composite plate with two continuous piezoelectric layers
4. Flat, rectangular, composite plate with piezoceramic patches
5. Composite cylindrical shell with one continuous piezoelectric layer

The numerical results generated by the SHAPE1 code were obtained using the material properties listed in Table 5.

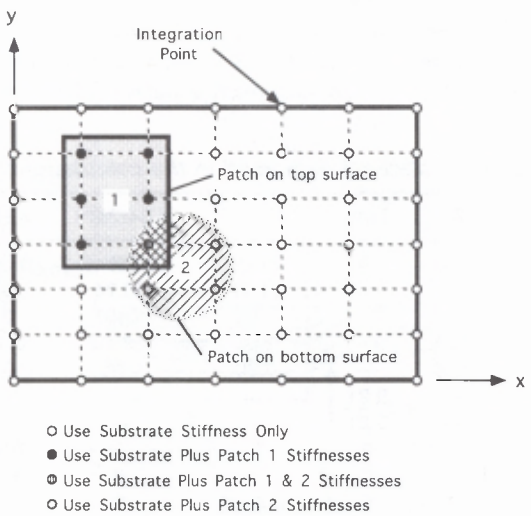

Figure 13. *Illustration of the integration points for numerical calculation of the integral over the domain.*

The piezoelectric film behaves in such a way that the relationship between induced strain and applied voltage is linear [42] [see Equation (11)] and may be characterized by two material constants d_{31} and d_{32}. The values of these properties for KYNAR piezoelectric film are given in Reference [42] and are included in Table 5.

The piezoceramic material behaves in such a way that the relationship between induced strain and applied voltage is nonlinear [see Equation (16)], and, by assuming isotropy, may be characterized by four material constants d_{31}, χ_{31}, ψ_1, and ψ_2 [see Equation (15)]. These constants were determined using the data of Crawley and Lazarus who generated these data for the specific purpose of obtaining the characteristics of the Piezoelectric Products G-1195 piezoceramic (Section 4 in Reference [13]). Crawley and Lazarus performed three tests, the first with an G-1195 unconstrained piezoceramic plate, the second with a G-1195 piezoceramic plate sandwiched between two aluminum plates, and the third with a G-1195 piezoceramic plate sandwiched between two orthotropic composite plates. We obtained the properties d_{31}, χ_{31}, ψ_1, and ψ_2 by matching the results generated by SHAPE1 to the data of Crawley and Lazarus for the above three configurations (Table 5).

Crawley and Lazarus measured in-plane strains on the surface of an unconstrained G-1195 piezoceramic plate. The results are shown in Figure 14. We calculated the strains for this G-1195 piezoceramic plate using the SHAPE1 code with the present four-parameter material model given by Equation (16). The results are included in Figure 14. As is seen the four-parameter model describes the data very accurately.

5.1 Cantilever, Sandwich Beam

We consider an 8.0 inch long and 1.0 inch wide cantilever beam consisting of a 0.60 inch thick isotropic core and two 0.35 inch thick aluminum face sheets (Figure 15). A load of $P = 100$ lbf is applied at the tip. The deflection along the

Table 5. Material data used in the calculations.

	Al	Core	T300/976	AS4/3501	KYNAR	G-1195
Thickness (in)	0.35	0.60	0.005	0.00545	0.00433	0.01
E_x (Msi)	10	—	21.75	20.74	0.29	9.137
E_y (Msi)	10	—	1.305	1.407	0.29	9.137
E_{xy} (Msi)	3.85	—	1.03	0.8702	0.1124	3.510
ν_{xy}	0.30	—	0.30	0.30	0.29	0.30
G_{xz} (Msi)	—	0.21	—	—	—	—
G_{yz} (Msi)	—	0.21	—	—	—	—
d_{31} (in/V $\times 10^{-9}$)	0	0	0	0	0.9055	10.4
d_{32} (in/V $\times 10^{-9}$)	0	0	0	0	0.1811	10.4
χ_{31} (in^2/V^2 $\times 10^{-15}$)	0	0	0	0	0	5.29
ψ_1 (in/V $\times 10^{-6}$)	0	0	0	0	0	25.2
ψ_2 (in/V $\times 10^{-6}$)	0	0	0	0	0	−6.40

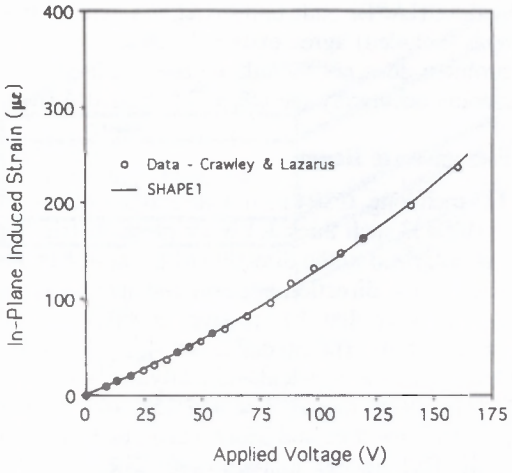

Figure 14. *Induced in-plane strain in an unconstrained G-1195 piezoceramic plate.*

length of the beam was calculated by the SHAPE1 code and by the model presented by Allen [32]. Note that the method for including the tip load in the analysis used by SHAPE1 is discussed in Appendix C. Allen's results were obtained both when shear deformation is present and when shear deformation is neglected inside the core. The calculated deflections are compared in Figure 15. The deflec-

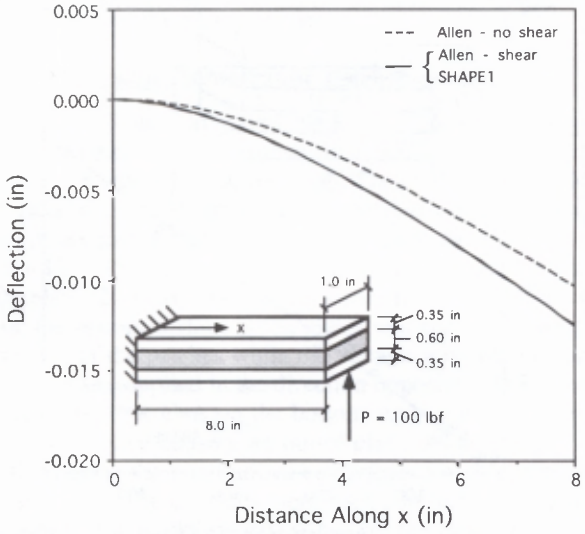

Figure 15. *Deflection along the length of a cantilever, sandwich beam. The 0.35 in face sheets are aluminum, and the 0.60 in core is aluminum honeycomb.*

tions calculated by the SHAPE1 code and by Allen's method (when shear deformation of the core is included) agree extremely closely.

Although this problem does not include piezoelectric effects, it demonstrates that SHAPE1 considers accurately the effects of shear deformation of the core.

5.2 Cantilever, Piezoelectric Beam

We consider a 3.15 inch long, 0.394 inch wide and 0.00866 inch thick cantilever beam made of two 0.00433 inch thick KYNAR piezoelectric film layers (Figure 16). The top layer is polarized in the direction of the applied voltage and the bottom layer is polarized in the direction opposite the applied voltage. A voltage is applied across the beam such that the top layer expands while the bottom layer contracts causing a deflection. The tip deflection was calculated by the SHAPE1 code. The tip deflection was also calculated analytically by Lee and Moon [14] using a Bernoulli-Euler beam model. Lee and Moon also reported experimentally measured tip deflections. Lee and Moon's analytical results and data as well as the results of SHAPE1 appear in Figure 16. The tip deflections given by SHAPE1 are in excellent agreement with Lee and Moon's experimental and analytical results.

5.3 Composite Plate

We consider a 6.0 inch by 4.0 inch T300/976 graphite/epoxy composite plate with a $[+30/-30]_s$ layup (Figure 17). There is a 0.004 inch thick continuous layer of KYNAR piezoelectric film bonded to the top and bottom surfaces. Each

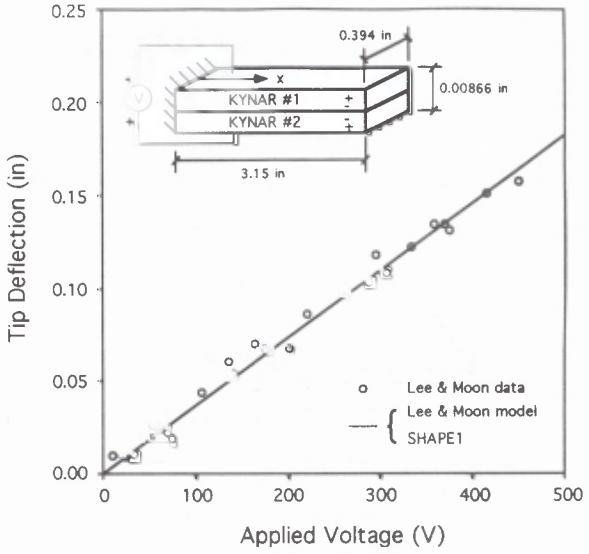

Figure 16. *Tip deflection of a cantilever, piezoelectric beam.*

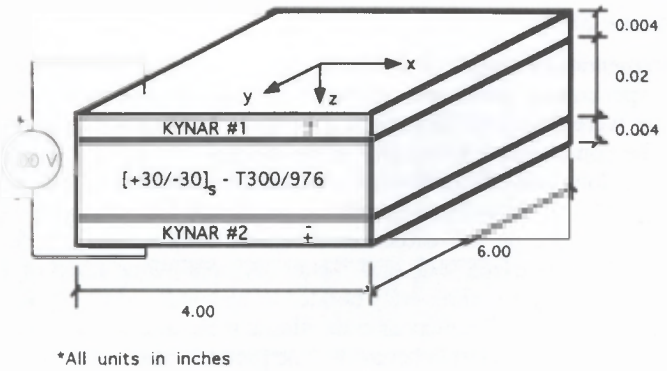

Figure 17. *Flat, rectangular, composite, piezoelectric plate.*

piezoelectric layer is mechanically isotropic but has orthotropic voltage versus strain behavior. The piezoelectric layers' orientations are such that the direction of largest strain is in the y-direction (see Figure 17). The top piezoelectric layer is polarized in the direction of the applied voltage and the bottom layer is polarized in the direction opposite the applied voltage. A voltage of 100 volts is applied across both films so that the plate is actuated in pure bending.

The deflections along the two perpendicular centerlines were calculated using the SHAPE1 code. The deflections were also calculated by an analytical plate solution described in Reference [33]. The results are presented in Figure 18. As can be seen, the deflections calculated by the SHAPE1 code agree extremely well with those calculated by the plate solution.

5.4 Composite Plate with Piezoceramic Patches

We consider an 11.5 inch long and 6.0 inch wide AS4/3501 graphite/epoxy composite plate (Figure 19). We investigated two plates: one with a $[0/+45/-45]_s$ layup and one with a $[+30_2/0]_s$ layup. The 0° direction is along the length of the plate. Isotropic G-1195 piezoceramic patches are applied on the top and bottom of the plates in the manner shown in Figure 19.

For the $[0/+45/-45]_s$ plate 100 volts was applied across the patches, and for the $[+30_2/0]_s$ plate 120 volts was applied across the patches. The voltage across the patches on the bottom surface of the plates was applied in the same direction as the polarization of the patches while the voltage across the patches on the top surface of the plate was applied in the direction opposite to the polarization of the patches. Therefore, the patches on the bottom surface expanded while those on the top surface contracted causing an out-of-plane deflection.

The deflections along the longitudinal centerline of both plates were calculated by the SHAPE1 code. These results were then compared in Figure 20 with the deflections given by the model proposed by and the experimental data obtained by Crawley and Lazarus [13]. The results in the figure show good agreement between the SHAPE1 code and the model and the data of Crawley and Lazarus.

5.5 Composite Shell

The aforementioned sample problems apply to flat beams and plates. No analytical or experimental results are available for the shape change of curved elements. Tests were therefore performed with a curved element to generate data which can be compared to the results of the model.

A 10.6 inch long and 6.0 inch wide rectangular shell was constructed of six layers of T300/976 unidirectional graphite/epoxy tape (Figure 21). The layup was $[90/+60/-60]_s$ with the 0° direction along the longitudinal direction. The radius of the inner surface was 12.0 inches. A continuous layer of KYNAR piezoelectric film [42] was adhesively bonded to the outer radius surface by Loctite DEPEND adhesive. The piezoelectric film is mechanically isotropic but has orthotropic voltage versus strain behavior. The piezoelectric layer's orientation is such that the direction of largest strain is in the lengthwise direction.

One of the corners of the shell was clamped. A voltage was applied across the film and the deflections of the two furthest corners were measured with a Schaevitz 100 HR-DC Linear Variable Differential Transducer (LVDT) (Figure 21). The deflections at the corners were also calculated by the SHAPE1 computer

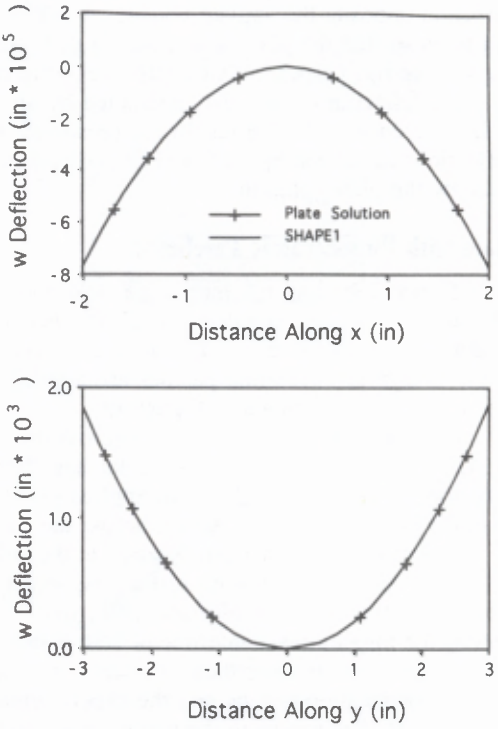

Figure 18. *Centerline deflections of a composite plate (see Figure 17).*

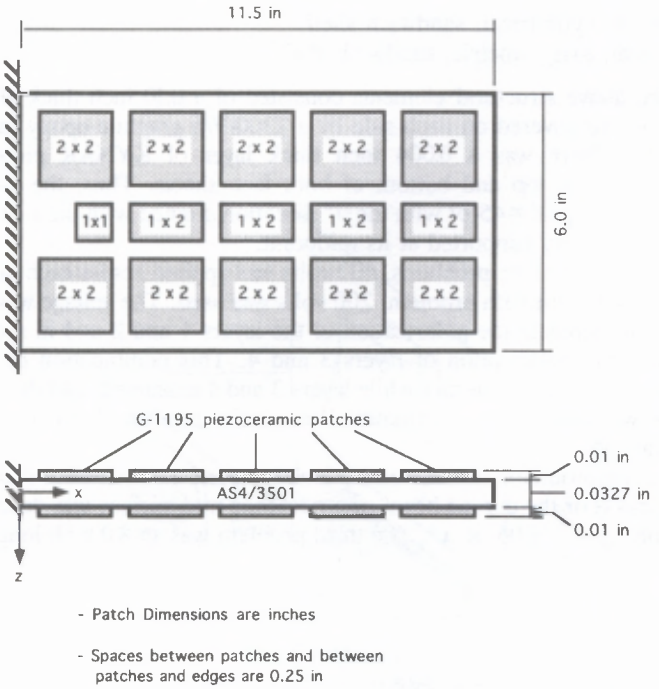

Figure 19. *Composite plate with G-1195 piezoceramic patches.*

code for different applied voltages. The numerical results and data are compared in Figure 22. Generally eight measurements were recorded at each corner for each voltage. At each voltage, the average of the measurements is represented by the circles in Figure 22 and the length of the error bars in the figure is two standard deviations. Again there is good agreement between the results of the SHAPE1 code and the data.

The aforementioned comparisons presented for the five problems show that, at least for these problems, the SHAPE1 code describes the changes in shape of plates and shells with good accuracy. These results lend confidence to the SHAPE1 code.

6. SAMPLE PROBLEMS

Solutions to sample problems were obtained to illustrate the capability of the SHAPE1 code and the type of results provided by the code. The following five cases were studied:

1. Straight, composite, sandwich beam
2. Curved, composite, sandwich beam
3. Flat, rectangular, composite, sandwich plate

4. Composite, cylindrical, sandwich shell
5. Composite, axisymmetric, sandwich shell

Each of the above structural elements consisted of a 0.10 inch thick aluminum honeycomb core covered on each side by a T300/976 graphite-epoxy face sheet (Figure 23). There was a 0.004 inch thick layer of KYNAR piezoelectric film placed on the top and bottom of both face sheets. Thus, the layup was [p/ ±45/0/p/core/p/0/ ∓45/p] with the 0° direction aligned with the x-axis. Each structure was rigidly supported at its midpoint.

In each of the first four problems, 400 volts was applied across each piezoelectric layer, while in the fifth problem, 200 volts was used. The voltage was applied in a direction opposite the polarization of the layers 1 and 2 and in a direction aligned with the polarization of layers 3 and 4. This combination of voltages caused layers 1 and 2 to contract while layers 3 and 4 expanded, and the resulting new shape was calculated. The material properties used in all calculations are listed in Table 5.

The first two problems considered 8.0 inch long and 1.0 inch wide straight and curved beams. For the curved beam, the reference mid-surface was described by the function $z_o = -0.05 \times x^2$. The third problem was an 8.0 inch long and 6.0

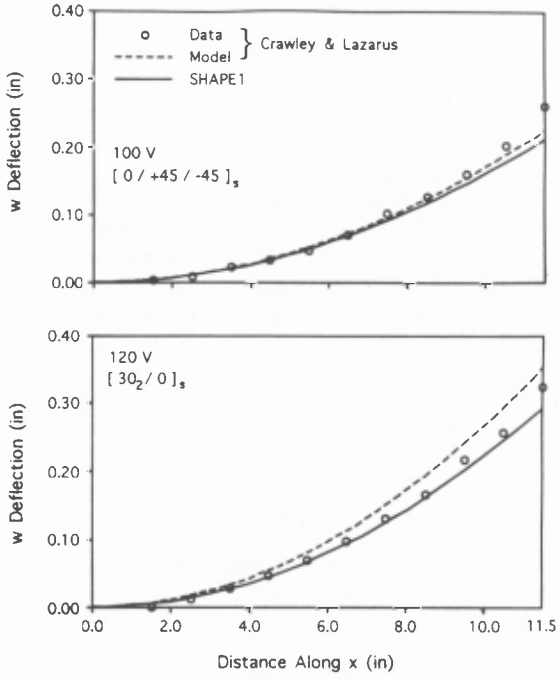

Figure 20. *Deflections along the longitudinal centerline of a composite plate with piezoceramic patches for two different lay-ups (see Figure 19).*

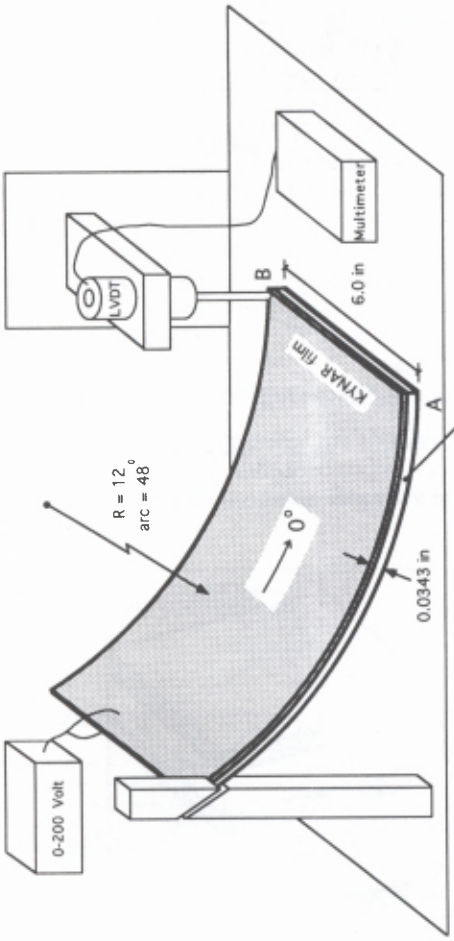

Figure 21. *Schematic of the experimental set-up.*

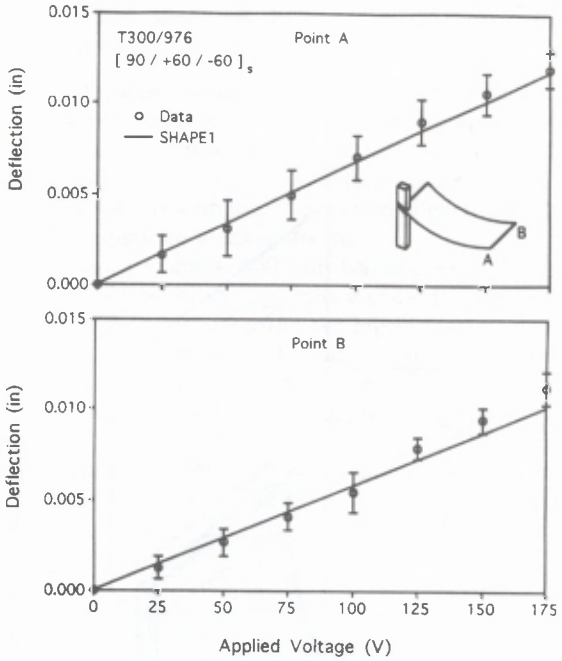

Figure 22. *Deflection at the remote corners of the composite shell (see Figure 21).*

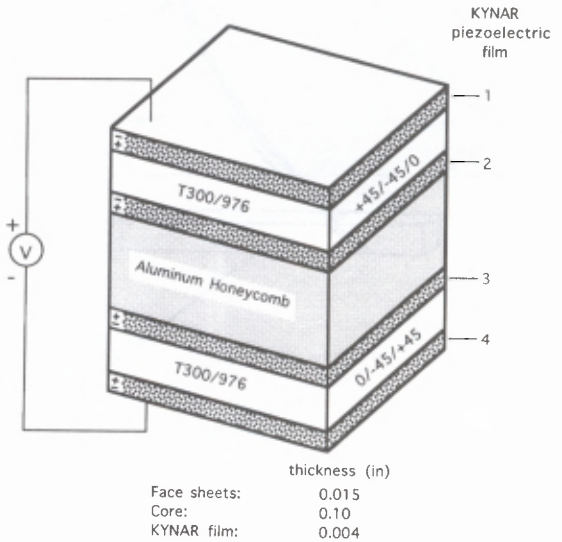

Figure 23. *Cross section of the sandwich construction used in the sample problems.*

inch wide flat plate, while the fourth problem was an 8.0 inch long and 6.0 inch wide cylindrical shell with the reference mid-surface described by the function $z_o = -0.05 \times x^2$. The fifth problem was an axisymmetric cap with reference mid-surface given by $z_o = -0.05 \times (x^2 + y^2)$. The shape changes of each of the above five structural elements are given in Figures 24 and 25.

In the aforementioned problems, it was assumed that the piezoelectric film was continuously covering the entire surface. To illustrate the use of the SHAPE1 code with patches, one sample problem was studied where the shape was changed by the use of piezoelectric patches. In this problem, the deflection of an 8.0 inch long and 1.0 inch wide straight beam was investigated. The cross section of the beam has an aluminum honeycomb core covered with T300/976 graphite-epoxy face sheets as shown in Figure 23, but without the KYNAR piezoelectric layers. Instead, two 2.0 inch long, 1.0 inch wide and 0.01 inch thick KYNAR piezoelectric patches were placed on the beam, as shown in Figure 26. Four hundred volts was applied to each patch in a direction opposite the polarization of the patch so that both patches contracted. The shape change caused by the application of this voltage is shown in Figure 26.

The results of the above sample problems illustrate the applicability of the SHAPE1 code to several geometries.

7. CONCLUDING REMARKS

A model was developed which describes the changes in shapes of composite beams, plates and shells containing embedded and surface mounted piezoelectric actuators. The model provides the changes in shape for specified applied voltages

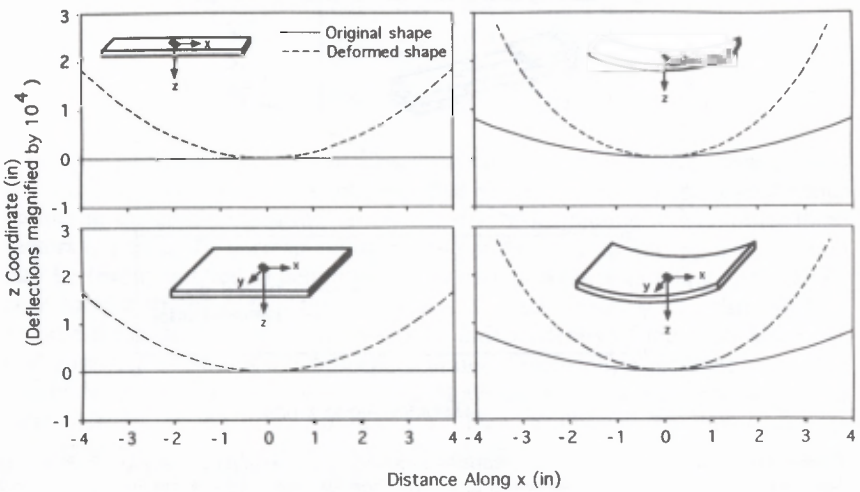

Figure 24. *Change in shape of a straight sandwich beam, a curved sandwich beam, a flat sandwich plate, and a cylindrical sandwich shell induced by applied voltage (see Figure 23 for element cross sections).*

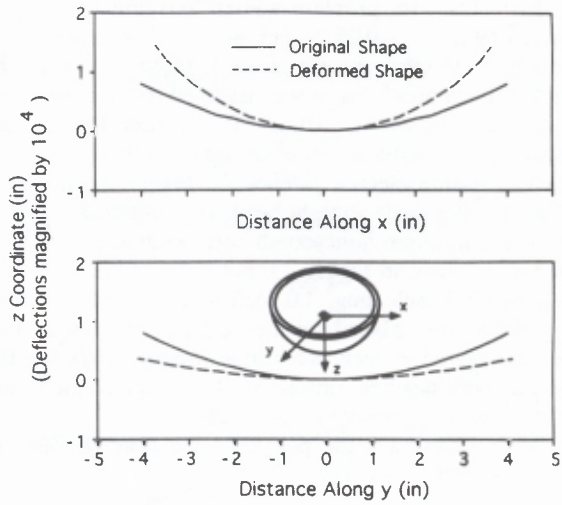

Figure 25. *Change in shape of an axisymmetric sandwich shell induced by applied voltage (see Figure 23 for element cross section).*

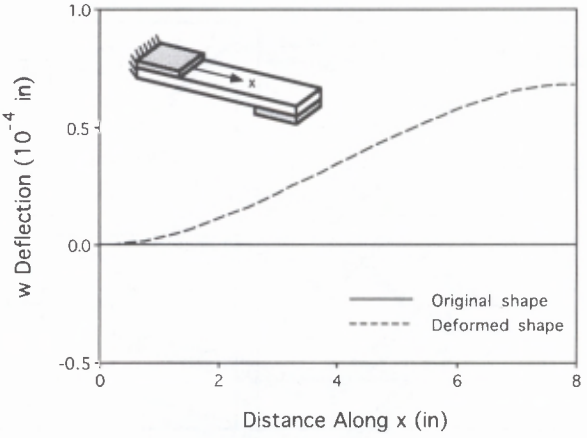

Figure 26. *Change in shape of a composite sandwich beam with piezoelectric patches. The face sheets are T300/976, the core is aluminum honeycomb, and the patches are KYNAR film.*

to the actuators. This information is needed in the design of piezoelectric actuator systems. In the design, parametric (sensitivity) studies are made with the SHAPE1 code, generating numerous results for different types, shapes, and locations of actuators. From these results, the actuator configuration which is most suitable for the given application is to be selected.

During field service, the voltages are needed which must be applied to achieve specified desired shapes. A model applicable to this problem is described in the companion paper [1].

APPENDIX A: THE SANDWICH STIFFNESS MATRIX

The element is of sandwich construction with thick faces consisting of two face sheets and a core (Figure 9). In the analysis the material is incompressible in the z-direction, and the core is "antiplane" (i.e., it resists no in-plane loads and has finite transverse shearing rigidity [32]). In addition, the transverse shear stress distribution existing in the faces is assumed to be linear (Figure A.1). Finally the face sheets behave as predicted by Classical Laminate Plate Theory [37].

The stiffness matrix for this sandwich construction $\mathbf{S}$ relates the combined strain vector $\boldsymbol{\epsilon}$ to the vector of force resultants $\mathbf{F}$ by [see Equation (8)]

$$\mathbf{F} = \mathbf{S}\boldsymbol{\epsilon} \tag{A.1}$$

or

$$\begin{Bmatrix} \mathbf{N} \\ \mathbf{M}_o \\ \mathbf{M}_l \\ \mathbf{Q} \end{Bmatrix} = \begin{bmatrix} \mathbf{S}_{11} & \mathbf{S}_{12} & \mathbf{S}_{13} & \mathbf{S}_{14} \\ \mathbf{S}_{21} & \mathbf{S}_{22} & \mathbf{S}_{23} & \mathbf{S}_{24} \\ \mathbf{S}_{31} & \mathbf{S}_{32} & \mathbf{S}_{33} & \mathbf{S}_{34} \\ \mathbf{S}_{41} & \mathbf{S}_{42} & \mathbf{S}_{43} & \mathbf{S}_{44} \end{bmatrix} \begin{Bmatrix} \boldsymbol{\epsilon}_o \\ \boldsymbol{\varkappa}_o \\ \boldsymbol{\varkappa} \\ \boldsymbol{\gamma} \end{Bmatrix} \tag{A.2}$$

In order to obtain the entries in the stiffness matrix a unit displacement method is used. The force resultants required to give a unit magnitude for one of the four vectors in the combined strain vector $\boldsymbol{\epsilon}$ and zero magnitude for the other three vectors in $\boldsymbol{\epsilon}$ gives the corresponding column of the stiffness matrix. This method may be readily applied to determine the entries in $\mathbf{S}$ corresponding to the reference surface strains $\boldsymbol{\epsilon}_o$ ($\mathbf{S}_{11}$ through $\mathbf{S}_{14}$) and shear strains $\boldsymbol{\gamma}$ ($\mathbf{S}_{14}$ through $\mathbf{S}_{44}$) because these strains may each be applied independently of the other strains in $\boldsymbol{\epsilon}$. Figure A.2 illustrates this procedure in one dimension to facilitate visualization of the physical processes occurring. However, $\boldsymbol{\varkappa}$ and $\boldsymbol{\varkappa}_o$ may not be applied independently of the other strains in $\boldsymbol{\epsilon}$. This result may be shown for the x-components of the curvature vectors by taking the first derivative with respect to x of the definition of γ_{xz} (Table 1)

$$\gamma_{xz} = \frac{\partial w}{\partial x} - \phi_x \tag{A.3}$$

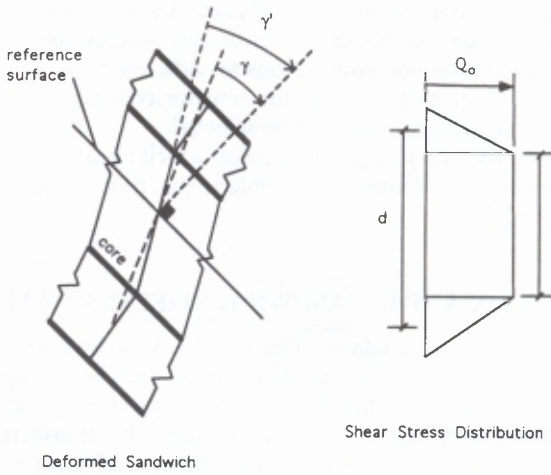

Figure A.1. *Shear stress distribution through the thickness of the sandwich.*

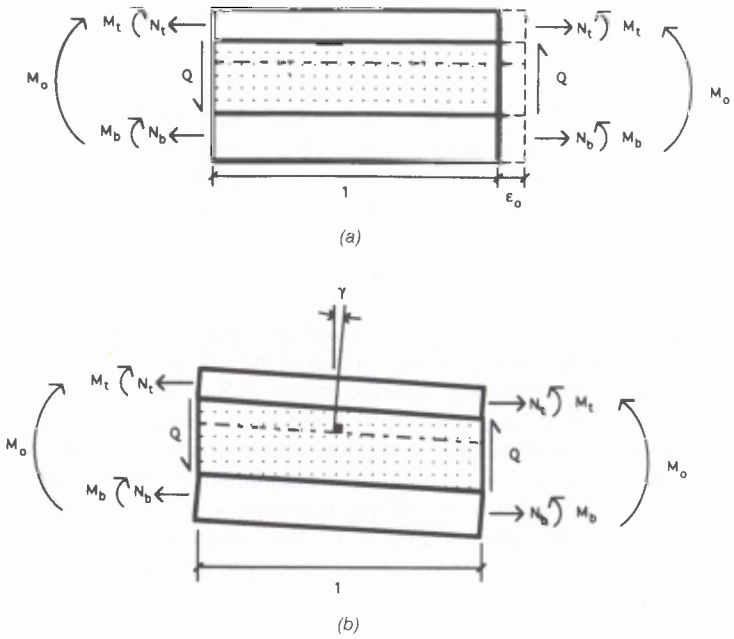

Figure A.2. *(a) Unit ϵ_x applied with all other strains held at zero. (b) Unit γ_{xz} applied with all other strains held at zero.*

which gives

$$\frac{\partial \gamma_{xz}}{\partial x} = \frac{\partial^2 w}{\partial x^2} - \frac{\partial \phi_x}{\partial x} = \varkappa_x - \varkappa_{ox} \tag{A.4}$$

Therefore, applying a unit $\boldsymbol{\varkappa}$ and keeping $\boldsymbol{\varkappa}_o$ zero implies the first derivative of $\boldsymbol{\gamma}$ is unity, and thus, $\boldsymbol{\gamma}$ varies linearly. A similar argument reveals that applying a unit $\boldsymbol{\varkappa}_o$ while keeping $\boldsymbol{\varkappa}$ zero must also be accompanied by a linear variation of $\boldsymbol{\gamma}$. These two configurations are shown in Figure A.3 also in one dimension only.

To determine the matrices making up the first column of $\mathbf{S}$, a unit $\boldsymbol{\epsilon}_o$ is applied while $\boldsymbol{\varkappa}_o$, $\boldsymbol{\varkappa}$, and $\boldsymbol{\gamma}$ are kept zero [Figure A.2(a)]. Physically this displacement field corresponds to in-plane stretching of the entire sandwich. Since the core is assumed to carry only transverse shear, the only nonzero force resultants required to hold this configuration are $\mathbf{N}$, $\mathbf{M}_o$, and $\mathbf{M}_l$. The following relations are obtained using force equilibrium relations

$$\mathbf{N} = (\mathbf{A}_t + \mathbf{A}_b)\boldsymbol{\epsilon} = \mathbf{S}_{11}\boldsymbol{\epsilon}_o \tag{A.5}$$

$$\mathbf{M}_o = (d_b\mathbf{A}_b - d_t\mathbf{A}_t)\boldsymbol{\epsilon} = \mathbf{S}_{21}\boldsymbol{\epsilon}_o \tag{A.6}$$

$$\mathbf{M}_l = (\mathbf{B}_t + \mathbf{B}_b)\boldsymbol{\epsilon} = \mathbf{S}_{31}\boldsymbol{\epsilon}_o \tag{A.7}$$

$$\mathbf{Q} = \mathbf{0} = \mathbf{S}_{41}\boldsymbol{\epsilon}_o \tag{A.8}$$

(see Section 3 for definitions of the symbols). Equations (A.5) through (A.8) provide $\mathbf{S}_{11}$, $\mathbf{S}_{21}$, $\mathbf{S}_{31}$ and $\mathbf{S}_{41}$ which comprise the first column of $\mathbf{S}$.

The matrices making up the fourth column of $\mathbf{S}$ are obtained by applying a unit $\boldsymbol{\gamma}$ while keeping $\boldsymbol{\epsilon}_o$, $\boldsymbol{\varkappa}_o$, and $\boldsymbol{\varkappa}$ zero [Figure A.2(b)]. This displacement field corresponds to a pure shearing of the core with no deformation of the face sheets. A distinction is made in the sandwich theory between γ and γ'. γ' is the shear strain of the core which is the angle between a line in the core which is originally normal to the reference surface and the normal to the deformed reference surface (Figure A.1). While γ, the shear strain of the sandwich, is defined as the angle between the line through the mid-surfaces of the two face sheets and the normal to the deformed reference surface. From equilibrium relations the shear stress resultant in the core $\mathbf{Q}_o$ is [32]

$$\mathbf{Q}_o = c\begin{bmatrix}\cos\theta & -\sin\theta \\ \sin\theta & \cos\theta\end{bmatrix}\begin{bmatrix}G_{13}^c & 0 \\ 0 & G_{23}^c\end{bmatrix}\begin{bmatrix}\cos\theta & \sin\theta \\ -\sin\theta & \cos\theta\end{bmatrix}\boldsymbol{\gamma}' \tag{A.9}$$

where θ is the orientation angle of the core principal axis and G_{13}^c and G_{23}^c are the on-axis transverse shear stiffnesses of the core in the 1-3 plane and the 2-3 plane, respectively (Figure 6). d is the distance between the midplane of the upper face sheet and the midplane of the lower face sheet, and c is the thickness of the core. It is desired to obtain the relation between the shear stress resultant for the sandwich $\mathbf{Q}$ and the rotation γ given the through-the-thickness shear stress distribu-

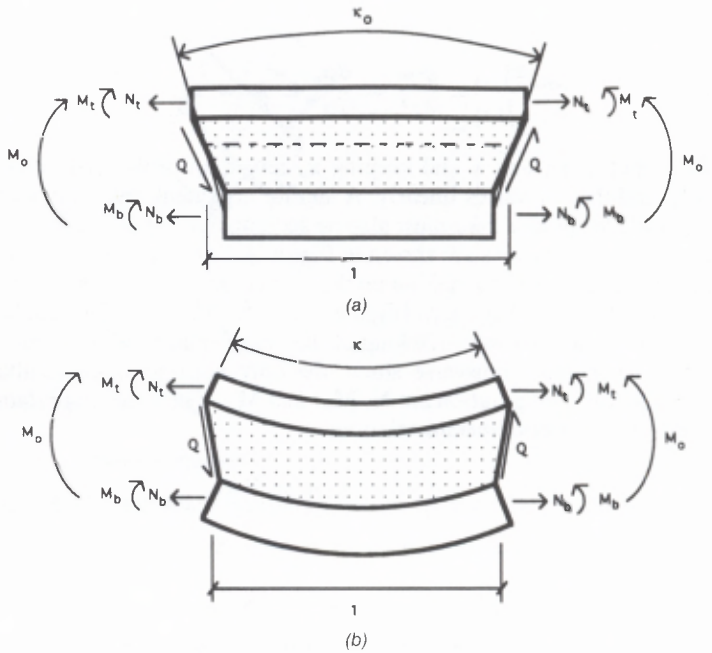

Figure A.3. *(a) Unit κ_{ox} applied with linear γ_{xz} and all other strains held at zero. (b) Unit κ_x applied with linear γ_{xz} and all other strains held at zero.*

tion shown in Figure A.1. Integrating through the thickness of the element, the sandwich shear stress is related to the core shear stress by

$$\mathbf{Q} = \frac{d}{c}\mathbf{Q}_o \tag{A.10}$$

By using small displacement approximations, the rotation γ is related to the rotation γ' by

$$\gamma = \frac{c}{d}\gamma' \tag{A.11}$$

The entries in the fourth column of the stiffness matrix are then obtained by substituting Equations (A.10) and (A.11) into Equation (A.9) and noting that the presence of a shear strain γ produces zero force resultants $\mathbf{N}$, $\mathbf{M}_o$ and $\mathbf{M}_t$. This gives

$$\mathbf{N} = \mathbf{0} = \mathbf{S}_{14}\boldsymbol{\gamma} \tag{A.12}$$

$$\mathbf{M}_o = \mathbf{0} = \mathbf{S}_{24}\boldsymbol{\gamma} \tag{A.13}$$

$$\mathbf{M}_l = \mathbf{0} = \mathbf{S}_{34}\boldsymbol{\gamma} \tag{A.14}$$

$$\mathbf{Q} = \frac{d^2}{c}\begin{bmatrix}\cos\theta & -\sin\theta \\ \sin\theta & \cos\theta\end{bmatrix}\begin{bmatrix}G^c_{13} & 0 \\ 0 & G^c_{23}\end{bmatrix}\begin{bmatrix}\cos\theta & \sin\theta \\ -\sin\theta & \cos\theta\end{bmatrix}\boldsymbol{\gamma} = \mathbf{S}_{44}\boldsymbol{\gamma} \tag{A.15}$$

Now the matrices in the second column of $\mathbf{S}$ may be obtained by applying a unit $\boldsymbol{\varkappa}_o$ while keeping $\boldsymbol{\epsilon}_o$ and $\boldsymbol{\varkappa}$ zero, and as discussed previously, applying a linear variation of $\boldsymbol{\gamma}$ [Figure A.3(a)]. This displacement field corresponds to a rotation of the midplanes of the core but no curvature change in the face sheets. From force equilibrium relations, keeping in mind that the presence of $\boldsymbol{\gamma}$ produces no resultant $\mathbf{N}$, $\mathbf{M}_o$, or $\mathbf{M}_l$, the following equations are obtained

$$\mathbf{N} = (d_b\mathbf{A}_b - d_t\mathbf{A}_t)\boldsymbol{\varkappa}_o = \mathbf{S}_{12}\boldsymbol{\varkappa}_o \tag{A.16}$$

$$\mathbf{M}_o = (d_t^2\mathbf{A}_t + d_b^2\mathbf{A}_b)\boldsymbol{\varkappa}_o = \mathbf{S}_{22}\boldsymbol{\varkappa}_o \tag{A.17}$$

$$\mathbf{M}_l = (d_b\mathbf{B}_b - d_t\mathbf{B}_t)\boldsymbol{\varkappa}_o = \mathbf{S}_{32}\boldsymbol{\varkappa}_o \tag{A.18}$$

$$\mathbf{Q} = \mathbf{S}_{42}\boldsymbol{\varkappa}_o + \mathbf{S}_{44}\boldsymbol{\gamma} \tag{A.19}$$

Equations (A.16) through (A.18) provide $\mathbf{S}_{12}$, $\mathbf{S}_{22}$, and $\mathbf{S}_{32}$ which, along with the fact that $\mathbf{S}_{42} = 0$ [Equation (A.13) and symmetry of $\mathbf{S}$], comprise the second column of $\mathbf{S}$.

Finally, the matrices in the third column are obtained by applying a unit $\boldsymbol{\varkappa}$ while keeping $\boldsymbol{\epsilon}_o$ and $\boldsymbol{\varkappa}_o$ zero, and as before, applying a linear variation of $\boldsymbol{\gamma}$ [Figure A.3(b)]. This displacement field corresponds to a constant curvature of the face sheets with zero overall curvature of the core (i.e., normals to the core reference surface remain vertical which implies that the core undergoes some shearing deformation). From force equilibrium equations the following equations are obtained

$$\mathbf{N} = (\mathbf{B}_t + \mathbf{B}_b)\boldsymbol{\varkappa} = \mathbf{S}_{13}\boldsymbol{\varkappa} \tag{A.20}$$

$$\mathbf{M}_o = (d_b\mathbf{B}_b - d_t\mathbf{B}_t)\boldsymbol{\varkappa} = \mathbf{S}_{23}\boldsymbol{\varkappa} \tag{A.21}$$

$$\mathbf{M}_l = (\mathbf{D}_t + \mathbf{D}_b)\boldsymbol{\varkappa} = \mathbf{S}_{33}\boldsymbol{\varkappa} \tag{A.22}$$

$$\mathbf{Q} = \mathbf{S}_{43}\boldsymbol{\varkappa} + \mathbf{S}_{44}\boldsymbol{\gamma} \tag{A.23}$$

Equations (A.20) through (A.22) provide $\mathbf{S}_{13}$, $\mathbf{S}_{23}$, and $\mathbf{S}_{33}$ which, along with the fact that $\mathbf{S}_{43} = 0$ [Equation (A.14) and symmetry of $\mathbf{S}$], comprise the third column of $\mathbf{S}$. Recall that from energy principles, the stiffness matrix relating the strains to the force resultants must be symmetric. Examination of the above derivation confirms that the matrix $\mathbf{S}$ is indeed symmetric.

For a core with no shear deformation or for a solid laminate, the stiffness matrix reduces to the classical stiffness matrix given in Reference [37].

$$\begin{Bmatrix} \mathbf{N} \\ \mathbf{M} \end{Bmatrix} = \begin{bmatrix} \mathbf{A} & \mathbf{B} \\ \mathbf{B} & \mathbf{D} \end{bmatrix} \begin{Bmatrix} \boldsymbol{\epsilon}_o \\ \boldsymbol{\varkappa} \end{Bmatrix} \tag{A.24}$$

where $\mathbf{A}$, $\mathbf{B}$, and $\mathbf{D}$ are the Classical Laminate Plate Theory stiffness matrices for the sandwich about a reference surface. This result may be shown as follows. In the present analysis the strains include transverse shear deformations in the curvatures $\boldsymbol{\varkappa}_o$ and shear strain in the core $\boldsymbol{\gamma}$. In the absence of these deformations, $\boldsymbol{\varkappa}$ and $\boldsymbol{\varkappa}_o$ are identical and $\boldsymbol{\gamma}$ is zero. Also, in the present analysis the moment resultant is split into two parts, the global moments $\mathbf{M}_o$ and the local moments $\mathbf{M}_l$, whose sum is the cross section moment resultant $\mathbf{M}$. Using the above information, Equation (A.2) may be rewritten

$$\begin{Bmatrix} \mathbf{N} \\ \mathbf{M}_o + \mathbf{M}_l \end{Bmatrix} = \begin{bmatrix} \mathbf{S}_{11} & \mathbf{S}_{12} + \mathbf{S}_{13} \\ \mathbf{S}_{21} + \mathbf{S}_{31} & \mathbf{S}_{22} + \mathbf{S}_{23} + \mathbf{S}_{32} + \mathbf{S}_{33} \end{bmatrix} \begin{Bmatrix} \boldsymbol{\epsilon}_o \\ \boldsymbol{\varkappa} \end{Bmatrix} \tag{A.25}$$

where $\boldsymbol{\gamma}$ and its corresponding entries in the stiffness matrix $\mathbf{S}$ have been removed since the former is zero.

Using the parallel axis theorem [37] to relate the stiffness matrices of the face sheets used in the present analysis to $\mathbf{A}$, $\mathbf{B}$, and $\mathbf{D}$ in Equation (A.24) yields the following

$$\begin{aligned} \mathbf{A} &= \mathbf{A}_t + \mathbf{A}_b \\ \mathbf{B} &= \mathbf{B}_t - d_t\mathbf{A}_t + \mathbf{B}_b + d_b\mathbf{A}_b \\ \mathbf{D} &= \mathbf{D}_t - 2d_t\mathbf{B}_t + d_t^2\mathbf{A}_t + \mathbf{D}_b + 2d_b\mathbf{B}_b + d_b^2\mathbf{A}_b \end{aligned} \tag{A.26}$$

By substituting the relations in Equation (A.26) into Equation (A.24) the resulting stiffness matrix $\mathbf{S}_{class}$ obtained using the analysis of Classical Laminate Plate Theory is

$$\mathbf{S}_{class} = \begin{bmatrix} \mathbf{A}_t + \mathbf{A}_b & \mathbf{B}_t - d_t\mathbf{A}_t + \mathbf{B}_b + d_b\mathbf{A}_b \\ \mathbf{B}_t - d_t\mathbf{A}_t + \mathbf{B}_b + d_b\mathbf{A}_b & \mathbf{D}_t - 2d_t\mathbf{B}_t + d_t^2\mathbf{A}_t + \mathbf{D}_b + 2d_b\mathbf{B}_b + d_b^2\mathbf{A}_b \end{bmatrix} \tag{A.27}$$

Now substitution of the previously developed expressions for the entries in the sandwich stiffness matrix $\mathbf{S}$ into Equation (A.25) gives

$$\mathbf{S}_{reduced} = \begin{bmatrix} \mathbf{A}_t + \mathbf{A}_b & \mathbf{B}_t - d_t\mathbf{A}_t + \mathbf{B}_b + d_b\mathbf{A}_b \\ \mathbf{B}_t - d_t\mathbf{A}_t + \mathbf{B}_b + d_b\mathbf{A}_b & \mathbf{D}_t - 2d_t\mathbf{B}_t + d_t^2\mathbf{A}_t + \mathbf{D}_b + 2d_b\mathbf{B}_b + d_b^2\mathbf{A}_b \end{bmatrix} \tag{A.28}$$

By comparing Equation (A.27) with Equation (A.28) it is evident that the classical stiffness matrix, $\mathbf{S}_{class}$, and the stiffness matrix of the present analysis reduced for the case where transverse shear deformations are absent, $\mathbf{S}_{reduced}$, are identical.

APPENDIX B: TRANSFORMATION MATRICES

The transformation matrix $\mathbf{T}_{ue}$ gives the combined strain vector ϵ when multiplied by the vector of unknown constants $\overline{\mathbf{C}}$

$$\epsilon = \mathbf{T}_{ue}\overline{\mathbf{C}} \tag{B.1}$$

where $\mathbf{T}_{ue}$ is given by

$$\mathbf{T}_{ue} = \begin{bmatrix} \dfrac{\partial \mathbf{f}}{\partial x} & \mathbf{0} & -\dfrac{\partial^2 z_o}{\partial x^2}\mathbf{h} & \mathbf{0} & \mathbf{0} \\ \mathbf{0} & \dfrac{\partial \mathbf{g}}{\partial y} & -\dfrac{\partial^2 z_o}{\partial y^2}\mathbf{h} & \mathbf{0} & \mathbf{0} \\ \dfrac{\partial \mathbf{f}}{\partial y} & \dfrac{\partial \mathbf{g}}{\partial x} & -2\dfrac{\partial^2 z_o}{\partial x \partial y}\mathbf{h} & \mathbf{0} & \mathbf{0} \\ \mathbf{0} & \mathbf{0} & \mathbf{0} & -\dfrac{\partial \mathbf{p}}{\partial x} & \mathbf{0} \\ \mathbf{0} & \mathbf{0} & \mathbf{0} & \mathbf{0} & -\dfrac{\partial \mathbf{r}}{\partial y} \\ \mathbf{0} & \mathbf{0} & \mathbf{0} & -\dfrac{\partial \mathbf{p}}{\partial y} & -\dfrac{\partial \mathbf{r}}{\partial x} \\ \mathbf{0} & \mathbf{0} & -\dfrac{\partial^2 \mathbf{h}}{\partial x^2} & \mathbf{0} & \mathbf{0} \\ \mathbf{0} & \mathbf{0} & -\dfrac{\partial^2 \mathbf{h}}{\partial y^2} & \mathbf{0} & \mathbf{0} \\ \mathbf{0} & \mathbf{0} & -2\dfrac{\partial^2 \mathbf{h}}{\partial x \partial y} & \mathbf{0} & \mathbf{0} \\ \mathbf{0} & \mathbf{0} & \dfrac{\partial \mathbf{h}}{\partial x} & -\mathbf{p} & \mathbf{0} \\ \mathbf{0} & \mathbf{0} & \dfrac{\partial \mathbf{h}}{\partial y} & \mathbf{0} & -\mathbf{r} \end{bmatrix} \tag{B.2}$$

In Equation (B.2), $\mathbf{f}$, $\mathbf{g}$, $\mathbf{h}$, $\mathbf{p}$, and $\mathbf{r}$ represent the trial functions used for the displacements u, v, w, ϕ_x, and ϕ_y, respectively (see Table 3).

The transformation matrix $\mathbf{T}_{ux}$ gives the displacements along an x = constant boundary $\mathbf{X}_b$ when multiplied by the vector of unknown constants $\overline{\mathbf{C}}$

$$\mathbf{X}_b = \mathbf{T}_{ux}\overline{\mathbf{C}} \tag{B.3}$$

where $\mathbf{T}_{ux}$ is given by

$$\mathbf{T}_{ux} = \begin{bmatrix} \mathbf{f} & \mathbf{0} & \mathbf{0} & \mathbf{0} & \mathbf{0} \\ \mathbf{0} & \mathbf{g} & \mathbf{0} & \mathbf{0} & \mathbf{0} \\ \mathbf{0} & \mathbf{0} & \mathbf{0} & \mathbf{p} & \mathbf{0} \\ \mathbf{0} & \mathbf{0} & \mathbf{0} & \mathbf{0} & \mathbf{r} \\ \mathbf{0} & \mathbf{0} & \dfrac{\partial \mathbf{h}}{\partial x} & \mathbf{0} & \mathbf{0} \\ \mathbf{0} & \mathbf{0} & \dfrac{\partial \mathbf{h}}{\partial y} & \mathbf{0} & \mathbf{0} \\ \mathbf{0} & \mathbf{0} & \mathbf{h} & \mathbf{0} & \mathbf{0} \end{bmatrix} \tag{B.4}$$

The transformation matrix $\mathbf{T}_{uy}$ gives the displacements along a y = constant boundary $\mathbf{Y}_b$ when multiplied by the vector of unknown constants $\overline{\mathbf{C}}$

$$\mathbf{Y}_b = \mathbf{T}_{uy}\overline{\mathbf{C}} \tag{B.5}$$

where $\mathbf{T}_{uy}$ is given by

$$\mathbf{T}_{uy} = \begin{bmatrix} \mathbf{0} & \mathbf{g} & \mathbf{0} & \mathbf{0} & \mathbf{0} \\ \mathbf{f} & \mathbf{0} & \mathbf{0} & \mathbf{0} & \mathbf{0} \\ \mathbf{0} & \mathbf{0} & \mathbf{0} & \mathbf{0} & \mathbf{r} \\ \mathbf{0} & \mathbf{0} & \mathbf{0} & \mathbf{p} & \mathbf{0} \\ \mathbf{0} & \mathbf{0} & \dfrac{\partial \mathbf{h}}{\partial y} & \mathbf{0} & \mathbf{0} \\ \mathbf{0} & \mathbf{0} & \dfrac{\partial \mathbf{h}}{\partial x} & \mathbf{0} & \mathbf{0} \\ \mathbf{0} & \mathbf{0} & \mathbf{h} & \mathbf{0} & \mathbf{0} \end{bmatrix} \tag{B.6}$$

APPENDIX C: BOUNDARY LOADS

C.1 Method of Analysis

Loads applied along the boundaries of the element may be included in the analysis by modifying Equation (27). The variation of the potential of the applied external forces δV_e may then be expressed as

$$\delta V_e = \delta V_{BC} + \delta V'_{BC} + \delta W_{BL} \tag{C.1}$$

where δV_{BC} and $\delta V'_{BC}$ are defined in Sections 3.4.1 and 3.4.2, respectively, and δW_{BL} represents the variation of the work done by external loads applied along the boundaries of the element. This work may be expressed in general for an arbitrary shaped element as [35]

$$\delta W_{BL} = \delta(\int \mathbf{U}_b \mathbf{F}_{b_{app}} dS) \tag{C.2}$$

where $\mathbf{F}_{b_{app}}$ and $\mathbf{U}_b$ represent the applied force resultants and the corresponding displacements along the boundary of the element and dS is an incremental length along the boundary.

For a rectangular element, the boundary consists of two sides along which x is constant and two sides along which y is constant (Figure C.1). In this case δW_{BL} is given by [35]

$$\begin{aligned} W_{BL} = &\left(\int_{y_1}^{y_2} \mathbf{X}_b^T \mathbf{F}_{x_{app}} dy \right) \text{along } x = x_1 \text{ and } x = x_2 \\ &+ \left(\int_{x_1}^{x_2} \mathbf{Y}_b^T \mathbf{F}_{y_{app}} dy \right) \text{along } y = y_1 \text{ and } y = y_2 \end{aligned} \tag{C.3}$$

where $\mathbf{F}_{x_{app}}$ and $\mathbf{X}_b$ are the force resultants applied and the displacements along

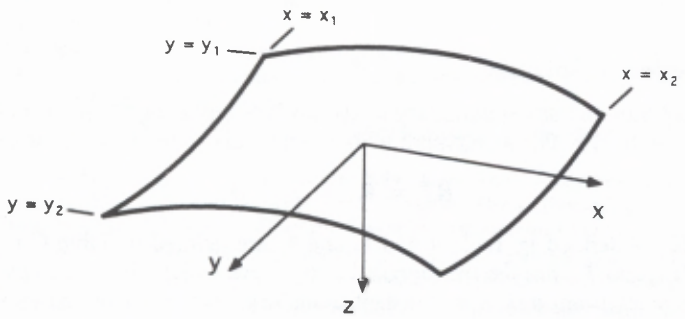

Figure C.1. *Illustration of the element boundaries for a rectangular element.*

Table C.1. Definitions of terms appearing in Equation (C.5).

Term	Origin	Definition
$\mathbf{I}_x$	x = constant boundary	$-\left(\int_{y_1}^{y_2} \mathbf{F}^T_{x_{app}} \mathbf{T}_{ux}\, dy\right)$ along $x = x_1$ and $x = x_2$
$\mathbf{I}_y$	y = constant boundary	$-\left(\int_{x_1}^{x_2} \mathbf{F}^T_{y_{app}} \mathbf{T}_{uy}\, dx\right)$ along $y = y_1$ and $y = y_2$

the x = constant boundaries, and $\mathbf{F}_{y_{app}}$ and $\mathbf{Y}_b$ are the corresponding values for the y = constant boundaries.

$$\mathbf{F}_{x_{app}} = \begin{Bmatrix} N_x \\ N_{xy} \\ M_{o_x} \\ M_{o_{xy}} \\ M_{l_x} \\ M_{l_{xy}} \\ Q_x \end{Bmatrix}, \quad \mathbf{X}_b = \begin{Bmatrix} u \\ v \\ \phi_x \\ \phi_y \\ \dfrac{\partial w}{\partial x} \\ \dfrac{\partial w}{\partial y} \\ w \end{Bmatrix}, \quad \mathbf{F}_{y_{app}} = \begin{Bmatrix} N_y \\ N_{xy} \\ M_{o_y} \\ M_{o_{xy}} \\ M_{l_y} \\ M_{l_{xy}} \\ Q_y \end{Bmatrix}, \quad \mathbf{Y}_b = \begin{Bmatrix} v \\ u \\ \phi_y \\ \phi_x \\ \dfrac{\partial w}{\partial y} \\ \dfrac{\partial w}{\partial x} \\ w \end{Bmatrix} \tag{C.4}$$

C.2 Method of Solution

The solution including boundary loads involves replacing the $\mathbf{R}_2$ term in Equation (32) with $\mathbf{R}_2^*$. For an element with a rectangular boundary, $\mathbf{R}_2^*$ is defined as

$$\mathbf{R}_2^* = \mathbf{R}_2 + \mathbf{I}_x + \mathbf{I}_y \tag{C.5}$$

where $\mathbf{R}_2$ is defined in Table 4 and $\mathbf{I}_x$ and $\mathbf{I}_y$ are defined in Table C.1. In these tables, $\mathbf{T}_{ux}$ and $\mathbf{T}_{uy}$ are the transformation matrices which give the displacements along x = constant and y = constant boundaries when multiplied by $\bar{\mathbf{C}}$, i.e.

$$\mathbf{X}_b = \mathbf{T}_{ux}\bar{\mathbf{C}} \qquad \mathbf{Y}_b = \mathbf{T}_{uy}\bar{\mathbf{C}} \tag{C.6}$$

The actual expressions for these transformation matrices appear in Appendix B. The unknown constants $\overline{\mathbf{C}}$ are evaluated as before using Equation (35) with $\mathbf{R}_2$ replaced by $\mathbf{R}_2^*$.

REFERENCES

1. Koconis, D. B., L. P. Kollár and G. S. Springer. 1994. "Shape Control of Composite Plates and Shells with Embedded Actuators. II. Desired Shape Specified," *Journal of Composite Materials,* 28(3):262–285.
2. Crawley, E. F. and J. de Luis. 1985. "Use of Piezo-Ceramics as Distributed Actuators in Large Space Structures," *Proceedings of the 26th AIAA/ASME/ASCE/AHS Structures, Structural Dynamics, and Materials Conf.*, pp. 126–133.
3. Crawley, E. F. and J. de Luis. 1987. "Use of Piezoelectric Actuators as Elements of Intelligent Structures," *AIAA Journal,* 25:1373–1385.
4. Bailey, T. and J. E. Hubbard. 1985. "Distributed Piezoelectric-Polymer Active Vibration Control of a Cantilever Beam," *Journal of Guidance and Control,* 8:605–611.
5. Burke, S. E. and J. E. Hubbard. 1987. "Active Vibration Control of a Simply Supported Beam Using a Spatially Distributed Actuator," *IEEE Control Systems Magazine,* 7:25–30.
6. Burke, S. E. and J. E. Hubbard. 1988. "Distributed Actuator Control Design for Flexible Beams," *Automatica,* 24:619–627.
7. Tzou, H. S. and G. C. Wan. 1990. "Distributed Structural Dynamics Control of Flexible Manipulators—I. Structural Dynamics and Distributed Viscoelastic Actuator," *Computers & Structures,* 35:669–678.
8. Tzou, H. S., C. I. Tseng and G. C. Wan. 1990. "Distributed Structural Dynamics Control of Flexible Manipulators—II. Distributed Sensor and Active Electromechanical Actuator," *Computers & Structures,* 35:679–687.
9. Cudney, H. H., D. J. Inman and Y. Oshman. 1990. "Distributed Structural Control Using Multilayered Piezoelectric Actuators," *Proceedings of the 31st AIAA/ASME/ASCE/AHS Structures, Structural Dynamics, and Materials Conf.*, pp. 2257–2264.
10. Cudney, H. H., D. J. Inman and Y. Oshman. 1989. "Distributed Parameters Actuators for Structural Control," *Proceedings of the 1989 American Control Conf.*, pp. 1189–1194.
11. Zhou, N., H. Sumali and H. H. Cudney. 1991. "Experimental Development of Piezofilm Modal Sensors and Characterization of Piezofilm Strain Rate Gages," *Proceedings of the 32nd AIAA/ASME/ASCE/AHS Structures, Structural Dynamics, and Materials Conf.*, pp. 735–743.
12. Hanagud, S., M. W. Obal and M. Meyyappa. 1985. "Electronic Damping Techniques and Active Vibration Control," *Proceedings of the 26th AIAA/ASME/ASCE/AHS Structures, Structural Dynamics, and Materials Conf.*, pp. 443–453.
13. Crawley, E. F. and K. B. Lazarus. 1989. "Induced Strain Actuation of Isotropic and Anisotropic Plates," *Proceedings of the 30th AIAA/ASME/ASCE/AHS Structures, Structural Dynamics, and Materials Conf.*, pp. 1451–1461.
14. Lee, C. K. 1990. "Theory of Laminated Piezoelectric Plates for the Design of Distributed Sensors/Actuators. Part I: Governing Equations and Reciprocal Relationships," *Journal of the Acoustical Society of America,* 87:1144–1158.
15. Lee, C. K. and F. C. Moon. 1990. "Modal Sensors/Actuators," *Journal of Applied Mechanics,* 57:434–441.
16. Lee, C. K., W.-W. Chiang and T. C. O'Sullivan. 1989. "Piezoelectric Modal Sensors and Actuators Achieving Critical Active Damping on a Cantilever Plate," *Proceedings of the 30th AIAA/ASME/ASCE/AHS Structures, Structural Dynamics, and Materials Conf.*, pp. 2018–2026.
17. Lee, C. K. and F. C. Moon. 1989. "Laminated Piezopolymer Plates for Torsion and Bending Sensors and Actuators," *Journal of the Acoustical Society of America,* 85:2432–2439.
18. Wang, B. T. and C. A. Rogers. 1991. "Modeling of Finite-Length Spatially Distributed Induced Strain Actuators for Laminate Beams and Plates," *Journal of Intelligent Material Systems and Structures,* 2:38–58.

19. 1991. Wang, B. T. and C. A. Rogers. 1991. "Laminated Plate Theory for Spatially Distributed Induced Strain Actuators," *Journal of Composite Materials*, 25:433–452.
20. Tzou, H. S. and J. P. Zhong. 1991. "Adaptive Piezoelectric Shell Structures: Theory and Experiment," *Proceedings of the 32nd AIAA/ASME/ASCE/AHS Structures, Structural Dynamics, and Materials Conf.*, pp. 2290–2296.
21. Tzou, H. S. and M. Gadre. 1989. "Theoretical Analysis of a Multi-Layered Thin Shell Coupled with Piezoelectric Shell Actuators for Distributed Vibration Controls," *Journal of Sound and Vibration*, 132:433–450.
22. Tzou, H. S. and C. I. Tseng. 1990. "Distributed Dynamic Identification and Controls of Flexible Shells: Theory and Finite Element Development," *Proceedings of the 31st AIAA/ASME/ASCE/AHS Structures, Structural Dynamics, and Materials Conf.*, pp. 2265–2273.
23. Tzou, H. S. 1991. "Distributed Modal Identification and Vibration Control of Continua: Theory and Applications," *Journal of Dynamic Systems, Measurement, and Control*, 113:494–499.
24. Jia, J. and C. A. Rogers. 1989. "Formulation of a Laminated Shell Theory Incorporating Embedded Distributed Actuators," in *Adaptive Structures*, B. K. Wada, ed., ASME Publication, AD-Vol. 15:103–113.
25. Ha, S. K., C. Keilers and F.-K. Chang. 1990. "Finite Element Analysis of Composite Structures Containing Distributed Piezoceramic Sensors and Actuators," *Proceedings of the 31st AIAA/ASME/ASCE/AHS Structures, Structural Dynamics, and Materials Conf.*, pp. 2323–2330.
26. Tzou, H. S. and C. I. Tseng. 1990. "Distributed Piezoelectric Sensor/Actuator Design for Dynamic Measurement/Control of Distributed Parameter Systems: A Piezoelectric Finite Element Approach," *Journal of Sound and Vibration*, 138:17–34.
27. Tzou, H. S. and C. I. Tseng. 1991. "Distributed Modal Identification and Vibration Control of Continua: Piezoelectric Finite Element Formulation and Analysis," *Journal of Dynamic Systems, Measurement, and Control*, 113:500–505.
28. Garba, J. A., B. K. Wada and J. L. Fanson. 1992. "Adaptive Structures for Precision Controlled Large Space Systems," *Journal of Intelligent Material Systems and Structures*, 3:348–366.
29. Chen, G.-S., C. P. Kuo and B. K. Wada. 1989. "Adaptive Structures for Precision Segmented Optical Systems," in *Adaptive Structures*, B. K. Wada, ed., ASME Publication, AD-Vol. 15:103–113.
30. Kuo, C. P. and B. K. Wada. 1989. "Composite Deformable Mirror," in *Active Telescope Systems*, F. J. Roddier, ed., SPIE Publication, 1114:495–505.
31. Flügge, W. 1973. *Stresses in Shells, Second Ed.* Springer-Verlag.
32. Allen, H. G. 1969. *Analysis and Design of Structural Sandwich Panels.* Pergamon Press.
33. Koconis, D. B. 1993. "Shape Control of Composite Plates and Shells Using Embedded Actuators," Ph.D. thesis, Stanford University.
34. Richards, T. H. 1977. *Energy Methods in Stress Analysis with an Introduction to Finite Element Techniques.* John Wiley & Sons.
35. Washizu, K. 1975. *Variational Methods in Elasticity and Plasticity, Second Ed.* Pergamon Press.
36. Kollár, L. P. 1990. "Buckling of Generally Anisotropic Shallow Sandwich Shells," *Journal of Reinforced Plastics and Composites*, 9:549–568.
37. Tsai, S. W. and H. T. Hahn. 1980. *Introduction to Composite Materials.* Lancaster, PA: Technomic Publishing Co., Inc.
38. Whitney, J. M. 1987. *Structural Analysis of Laminated Anisotropic Plates.* Lancaster, PA: Technomic Publishing Co., Inc.
39. Akin, J. E. 1982. *Application and Implementation of Finite Element Methods.* Academic Press.
40. Timoshenko, S. and S. Woinowsky-Krieger. 1959. *Theory of Plates and Shells, Second Ed.* McGraw-Hill Book Co.
41. Abramowitz, M. and I. Stegun. 1972. *Handbook of Mathematical Functions with Formulas, Graphs, and Mathematical Tables, Tenth Ed.* Dover Publications.
42. 1987. "Properties of KYNAR Piezo Film," in *KYNAR Pizeo Film Technical Manual*. Valley Forge, PA: ATOCHEM, pp. 9–20.